Available online at www.sciencedirect.com

ScienceDirect

Geochimica et Cosmochimica Acta 282 (2020) 1–18

Geochimica et Cosmochimica Acta

www.elsevier.com/locate/gca

Spatial and temporal heterogeneity of geochemical controls on carbon cycling in a tidal salt marsh

Angelia L. Seyfferth [a,b,*], Frances Bothfeld [a], Rodrigo Vargas [a], Jason W. Stuckey [a,c], Jian Wang [d], Kelli Kearns [a,e,f], Holly A. Michael [b,e], Julia Guimond [b], Xuan Yu [b,g], Donald L. Sparks [a]

[a] *Department of Plant and Soil Sciences, University of Delaware, USA*
[b] *Department of Geological Sciences, University of Delaware, USA*
[c] *Department of Biology and Environmental Science Program, Multnomah University, USA*
[d] *Canadian Light Source Inc., University of Saskatchewan, Canada*
[e] *Department of Civil and Environmental Engineering, University of Delaware, USA*
[f] *Environmental Resources Management, USA*
[g] *School of Civil Engineering, Sun Yat-sen University, China*

Received 5 September 2019; accepted in revised form 13 May 2020; available online 22 May 2020

Abstract

Tidal salt marsh ecosystems store copious amounts of carbon (C) within sediments. In order to predict how these C stores may be affected by environmental change, it is critical to assess current CO_2 and CH_4 production and efflux from these ecosystems. Production and efflux of these greenhouse gases (GHGs) are governed by coupled geochemical, hydrological, physical and biological processes in sediments that are sensitive to local conditions, which can result in large spatial and temporal heterogeneity of GHGs dynamics within the ecosystem. To understand how the drivers of GHGs dynamics vary across salt marsh ecosystems, we coupled solid-phase geochemistry to measurements of porewater chemistry (to ~1 m), CO_2 and CH_4 production in sediments and efflux to the atmosphere in a temperate tidal salt marsh for over one year to capture seasonal patterns within two vegetation zones of the marsh landscape that have distinct biogeochemical and hydrologic conditions: Tall *Spartina* (TS) and Short *Spartina* (SS). The SS vegetation zone experienced nearly constant inundation, low redox values (−200 to 200 mV), porewater pH 6–7 that did not vary with depth or time, an enrichment of pyrite and goethite with depth and up to 3 mM porewater sulfide. In contrast, the TS vegetation zone on the natural levee proximal to a tidal channel experienced large water level oscillations due to spring-neap tides that resulted in variable but higher redox values (0–700 mV), porewater pH 6–7 at depth but surface (0–3 cm) as low as 4 in the spring, an enrichment of ferrihydrite and a depletion of pyrite at ~30 cm, and up to 0.8 mM ferrous Fe in porewater. At 50–56 cm, solid phase analyses (STXM-NEXAFS) revealed differential C speciation between the two vegetation zones, with stronger C-Fe spatial association at TS and stronger C-Ca co-association at SS despite both having similar soil pH of 3–4. These results suggest that soil pH may not be strongly predictive of C-mineral control in flooded marsh sediments. Both vegetation zones showed consistent CO_2 and CH_4 emissions from sediments to the atmosphere throughout the study period with TS having ~60% higher median CO_2 and SS having ~55% higher median CH_4 efflux. Using depth profiling, unexpectedly high concentrations of CO_2 (>200 μM) and CH_4 (>200 μM) were observed at depths 50–75 cm at both zones that were higher for SS in these sulfate-rich (up to 17 mM) sediments, which suggests methylotrophic methanogenesis occurs deep within the profile of salt marsh sediments away from the tidal channel. Moreover, if we extrapolate our median depth values of CH_4 and CO_2 to the 5.3 Mha of global salt marshes, this could

* Corresponding author at: 531 S. College Avenue, 152 Townsend Hall, Newark, DE 19711, USA.
E-mail address: angelias@udel.edu (A.L. Seyfferth).

https://doi.org/10.1016/j.gca.2020.05.013

account for a conservative estimate of ~70 Gg of unaccounted C stored in gaseous form (i.e., CH_4 and CO_2) in marsh sediments, which should be considered when attempting to understand the current patterns and future responses of carbon dynamics from these ecosystems.

Keywords: CH_4; CO_2; Fluxes; STXM-NEXAFS; X-ray diffraction; Redox; Fe EXAFS

1. INTRODUCTION

Tidal salt marsh ecosystems store 1–3 orders of magnitude more carbon in sediments (~218 g C m^{-2} yr^{-1}) than freshwater wetlands (20–30 g C m^{-2} yr^{-1}) or forests (0.7–55 g C m^{-2} yr^{-1}) (Roulet, 2000; Chmura et al., 2003; Mcleod et al., 2011), yet can also release a wide range of carbon dioxide (CO_2, 100–10,000 g m^{-2} yr^{-1}) and methane (CH_4, 0.5–22 g m^{-2} yr^{-1}) greenhouse gases (GHGs) to the atmosphere (Bartlett et al., 1987; Magenheimer et al., 1996; Liu et al., 2019; Cao et al., 2020). Past research indicated that while salt marshes have sustained efflux of CO_2 to the atmosphere, they may not be substantial sources of CH_4 (Chmura et al., 2003; Poffenbarger et al., 2011) due to the inhibitory effects of bacterial sulfate (SO_4^{2-}) reduction on methanogenesis (Kristjansson et al., 1982; Lovley and Phillips, 1987; Kuivila et al., 1989). Supporting this paradigm is the inverse relationship found between concentrations of porewater sulfate and CH_4 or porewater salinity and CH_4 efflux from variable salinity marshes, with near complete cessation of CH_4 production or efflux above 8 mM sulfate and 15‰ salinity (Poffenbarger et al., 2011). In contrast, others have shown that salinity higher than 9‰ does not necessarily inhibit CH_4 production (King and Wiebe, 1978; Van Der Nat and Middelburg, 2000; Weston et al., 2006; Middelburg et al., 2014; Wilson et al., 2015; Xiao et al., 2018). Emerging evidence from a variety of environments from forests to wetlands supports the idea that the heterogeneity of the soil/sediment environment creates microenvironments that can support seemingly exclusive microbial metabolisms in close proximity to each other (Bethke et al., 2011) and therefore affect biogeochemical processes. Examples include the 'methane paradox' with methanogenic activity occurring in microsites in otherwise oxic soil and water environments (Teh and Silver, 2006; Darling and Gooddy, 2006; Angle et al., 2017), reducing conditions in soil aggregate interiors in otherwise oxic environments (Silver et al., 1999; Pallud et al., 2010; Masue-Slowey et al., 2011; Ying et al., 2013; Keiluweit et al., 2017), and simultaneous sulfate reduction and methanogenesis (Oremland et al., 1982; Senior et al., 1982; Postma and Jakobsen, 1996; Le and Roger, 2010; Segarra et al., 2013).

It is becoming clear that while sulfate-reducing bacteria can outcompete methanogens for substrate during hydrogenotrophic and aceticlastic methanogenesis, methylotrophic methanogenesis may be the dominant pathway for CH_4 production in sulfate-rich sediments (Oremland et al., 1982; Xiao et al., 2018; Jones et al., 2019). Methylotrophic methanogenesis can proceed through fermentation of methylated compounds such as methanol, methylsulfides or methylamines, and sulfate-reducing bacteria do not compete for substrate. In fact, sulfate-reducing bacteria and fermentive bacteria have been shown to be synergistic in the breakdown of glycine betaine (GBT) to form trimethylamine (TMA), which can then be used methanogens to form CH_4 (Hippe et al., 1979; Oremland et al., 1982; King, 1984; Jones et al., 2019), but CH_4 production can also proceed via direct demethylation of GBT (Watkins et al., 2014; Ticak et al., 2015). Because methanogenesis can co-occur in environments dominated by sulfate reduction, this warrants a closer look at the role of tidal salt marsh ecosystems in CH_4 production and efflux to the atmosphere in the context of local-to-global environmental change (IPCC, 2014; Hayes et al., 2018).

Not only is the soil environment heterogeneous on the micro-scale, but tidal marshes are heterogeneous on the ecosystem-scale both spatially and temporally, and this heterogeneity should be considered when modeling multi-scale C dynamics. Past research has focused predominantly on discrete measurements of either CO_2 or CH_4 efflux from sediments to the atmosphere in specific areas of tidal marshes (Reid et al., 2013) or at the ecosystem-scale for CO_2 and CH_4 using the eddy covariance technique (Knox et al., 2019). Researchers using these approaches have recognized that there is a need to resolve specific landscape contributions and the underlying biogeochemical processes for CO_2 or CH_4 dynamics (Waddington and Roulet, 1996; Fagherazzi et al., 2013; Tong et al., 2013; Reid et al., 2013). Previous studies in peatlands and wetlands found that water table depth is a primary driver of CO_2 and CH_4 production due to the effect of inundation on biogeochemistry, specifically redox conditions (Moore and Dalva, 1993; Moore and Roulet, 1993; Kelley et al., 1995; Wachinger et al., 2000; Smith et al., 2003). Peatlands and wetlands have similar water table depth variations (0–60 cm) (Le and Roger, 2010) to tidal salt marshes (Wolanski, 2007). However, water table elevations in tidal marshes fluctuate diurnally due to tidal patterns and can be highly variable across the ecosystem, causing CO_2 and CH_4 production, as well as efflux rates, to have both seasonal and diurnal patterns (Bartlett et al., 1985; Chanton et al., 1989; Kelley et al., 1995; Yang and Chang, 1998; Maher et al., 2015; Villa et al., 2019). Tidal influence is also variable across the marsh landscape due to differences in topography and proximity to tidal channels (Drabsch et al., 1999). Water table variations can range from daily swings in the water table caused by tides (~50 cm), to no daily variation in water table (Drabsch et al., 1999; Montalto et al., 2007) depending on the ecological zone within a marsh. However, even in areas with little to no daily variations, there can be longer scale variations caused by spring-neap tidal cycles.

Differing water table dynamics across tidal salt marshes lead to spatial heterogeneity of biogeochemical processes that affect CO_2 and CH_4 production and efflux. Tides affect the balance of CO_2 and CH_4 production by impacting microbial activity through changes in dissolved oxygen, dissolved organic carbon (DOC), and terminal electron acceptor (TEA) concentrations in sediment porewaters. For example, the incoming tide is a source of DOC (Hemminga et al., 1992; Hemminga et al., 1993), which provides energy for microbial activity and is often the rate-limiting component in microbial respiration (Winfrey and Zeikus 1977; Holmer and Kristensen, 1994). The incoming tide is also a source of SO_4^{2-} that may locally stimulate sulfate-reducing bacteria (SRB), which may compete with methanogens and therefore result in more CO_2 and less CH_4 production (Weston et al., 2010). Furthermore, the outgoing tide can drain portions of the marsh enough to oxygenate the sediments and 'shock' the microbial activity and allow O_2 to re-oxidize some spent TEAs, and thus replenish the supply of TEAs for microbial respiration (Kelley et al., 1995; Segers, 1998; Smith et al., 2003). During periods of inundation, CO_2 and CH_4 produced within the soil column have limited conduits to escape to the atmosphere through sediment pore spaces, and could become trapped within the soil column, especially if the GHGs are produced below the rooting depth of the dominant vegetation, as aerenchyma can act as a conduit for GHGs to escape (Kludze et al., 1993). However, large water table elevation oscillations may allow trapped GHGs to escape, and tidal pumping may laterally transport dissolved GHGs into tidal channels (Trifunovic et al., 2018). Both dissolved CH_4 and CO_2 concentrations have an inverse relationship with tidal amplitude, indicating a flushing effect with low tide (Beck et al., 2008; Grunwald et al., 2009; Tong et al., 2013; Call et al., 2015). However, these previous studies are limited to dissolved CO_2 and CH_4 near or in tidal channels and do not quantify CO_2 or CH_4 gas production with depth and efflux from sediments across the marsh landscape over seasons. We reason that there is a potential for large CO_2 and CH_4 efflux rates directly from sediments in a marsh during tidal cycles, or tidal pumping events, because the absence of inundation during low tide can allow for GHGs trapped deeper in the sediment profile to rapidly escape to the atmosphere.

Here, we aimed to understand how biogeochemical and water table elevation spatial gradients affect CH_4 and CO_2 production and efflux in a temperate tidal salt marsh. We evaluated the temporal and spatial heterogeneity of biogeochemical cycling of redox-sensitive parameters and CO_2 and CH_4 production and efflux across the tidal marsh landscape. We hypothesized that 1) vegetation zones on the natural levee proximal to the tidal channel will have a greater change in water level resulting in more oxidizing sediments than zones farther from the tidal channel; and 2) vegetation zones with greater change in water table elevation will have a higher rate of C efflux than those with less variation in water table elevation. The novelty of this study is that we coupled biometeorological information of CH_4 and CO_2 dynamics with solid-phase geochemistry, hydrologic measurements, and porewater chemistry to provide insights about the biogeochemical controls of C dynamics across a temperate tidal marsh landscape.

2. METHODS

2.1. Site Description

This study took place in the St. Jones Reserve, a coastal estuary southwest of Dover, Delaware (Fig. 1). The St. Jones is part of the National Estuarine Research Reserve System (NERRS) and is managed by the Delaware Department of Natural Resources and Environmental Control (DNREC). The St. Jones Reserve is 15.2 km^2 with an 8.8 km stretch of medium salinity (~8–25 ‰) tidal river (Capooci et al., 2019). This river is a tributary of the St. Jones River that drains agricultural land but also experiences tidal inundation from the Delaware Bay, as the St. Jones River is a tributary of the Delaware Bay. This region experiences a temperate climate with average temperature ranging from 0 °C in the winter to 25 °C in the summer with a yearly average temperature of 15 °C, and receives about 100 cm annual precipitation (Fig. 2a). High tides occur twice daily with amplitudes ranging from ~1 m to ~1.5 m during neap and spring tides, respectively (Fig. 2b).

The reserve has continuous monitoring of meteorological data managed by the Delaware Environmental Observation System (DEOS), and water quality data that includes salinity, water temperature, conductivity, pH, turbidity, and dissolved oxygen managed by DNREC. There is also a USGS tidal gauge (01483700) monitoring system approximately 20 km upstream of the mouth of the St. Jones River and managed by the MD-DE-DC Water Science Center Dover office that we used for tidal amplitudes.

To capture spatial heterogeneity of the marsh, we focused our study on two vegetation zones (Fig. 1) across the marsh landscape: Tall Spartina (TS), proximal to the main tidal channel on the natural levee and dominated by the tall form of *Spartina alterniflora* L. (saltmarsh cordgrass) with patches of *S. cynosuriodes* L. (big cordgrass), and Short Spartina (SS), approximately 70 m from the main tidal channel and dominated by the short form of *S. alterniflora* L. with patches of *S. patens L.* (saltmeadow cordgrass).

2.2. Sediment Cores and Characterization

A 90 cm sediment core was taken at each zone in June 2014. We found that SS had 5 distinct horizons and TS had 3 horizons up to 89 cm depth (Table 1). The sediment cores were sectioned into three sections (0–27, 27–73, 73+ cm) for TS and 5 sections (0–19, 19–38, 38–50, 50–66, 66 + cm) for SS corresponding to sediment horizon locations (Fig. S1), and each section was heat-sealed inside of gas-impermeable bags outfitted with oxygen scrubbers (Mitsubishi Anaero-Pack-Anaero) during transport to the laboratory.

Sediment from each horizon was subsampled for solid phase characterization under anoxic conditions. An intact ~1 cm^3 portion of each horizon was dried at ambient laboratory temperature under anoxic conditions and reserved

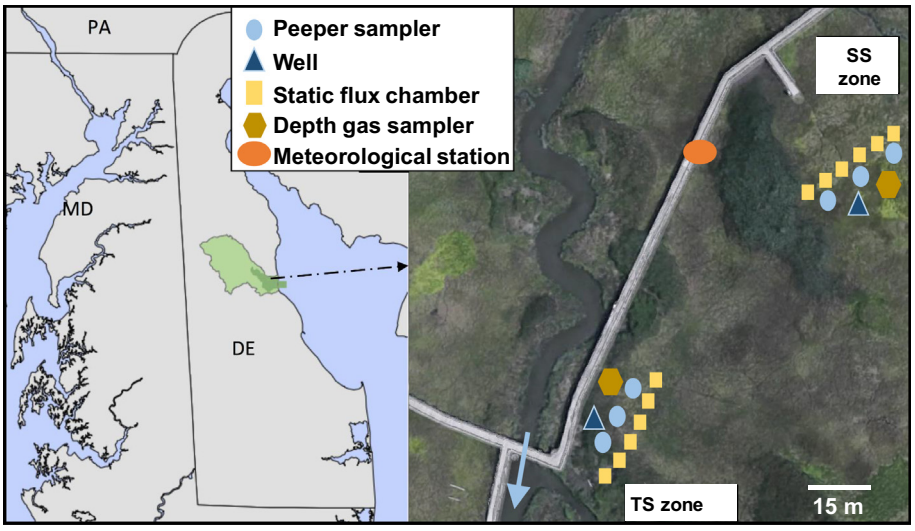

Fig. 1. Study site location at the St. Jones Reserve near Dover, DE. Map of Delaware and surrounding states with the St. Jones River watershed highlighted in light green (left), and a Google image showing the Tall *Spartina* (TS) and Short *Spartina* (SS) vegetation zones equipped with water and gas sampling devices (right). The arrow represents the outgoing flow of tidal channel water.

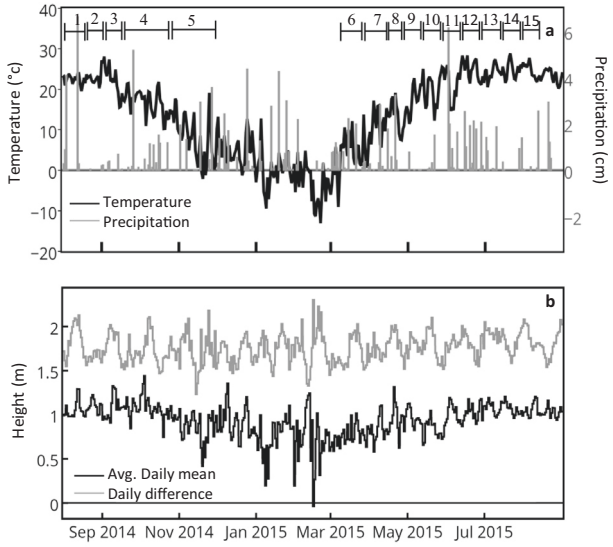

Fig. 2. Average daily temperature (black) and precipitation (grey) at the St. Jones Reserve over the 15 sampling periods labeled 1–15 (a) and average daily mean (black) and daily difference between high and low tide (grey) in the St. Jones River (b). Numbers 1–15 in panel (a) correspond to equilibrium time for peeper sampling events reported in Fig. 3 and Supporting Fig. S3.

for X-ray imaging and C speciation analysis using STXM-NEXAFS (see Section 2.4). A portion of each horizon was composited and sieved to 2 mm for analysis of pH (1:1 water extraction). A portion of the sieved sample was powdered and used for CNS analysis (Elementar Cube), X-ray diffraction (Bruker), and bulk Fe EXAFS (described in the next section). A portion of the sieved sediment was further sieved to 0.15 mm for ammonium oxalate (AAO) extraction to target poorly-crystalline Fe (McKeague and Day, 1966) and further sieved to 0.053 mm for citrate-bicarbonate-dithionite (CBD) extractions to target total free Fe (Mehra, 1958). All extracts were analyzed for total elements using ICP-OES (Thermo Elemental Intrepid II XSP Duo View).

2.3. Fe EXAFS

Four powdered sediment samples collected from the SS zone at −7, −30, −50, and −70 cm and three from the TS zone at −10, −30, and −80 cm relative to the sediment surface were used for bulk Fe EXAFS. Bulk Fe EXAFS was conducted at the Stanford Synchrotron Radiation Lightsource on beamline 11–2, which is equipped with a Si 2 2 0 (phi 90) LN2-cooled double crystal monochromator and Kirkpatrick-Baez mirrors. The incident beam was detuned to 50% to minimize harmonics and the energy was calibrated using a standard Fe foil to the first Fe inflection point at 7112 eV. Iron K-edge spectra were obtained from 150 eV below the edge to k values of 13 $Å^{-1}$ and fluorescence was monitored with a Lytle detector. Four spectra were obtained per sample and were averaged, background subtracted, normalized, fit with a spline function (k-weight = 3). These normalized spectra were fit by linear combination using ferrihydrite, goethite, mackinawite, siderite, pyrite and vivianite as standards (Hansel et al., 2003).

2.4. STXM-NEXAFS

Sediment samples at depths of 50 and 56 cm were chosen for STXM-NEXAFS analysis from TS and SS, respectively. Field moist samples that had been sealed under anoxic conditions with oxygen scrubbers (Mitsubishi Anaero-Pack-Anaero) during the transport to the lab were allowed to dry in an anoxic glovebox (95% N_2/5% H_2 atmosphere). Visible roots and plant material were removed by hand. Dry sediments were stored and shipped in an anoxic

Table 1
Soil chemical properties of composite sediment horizons at the SS and TS zones at the St. Jones Reserve. AAO = ammonium oxalate extractable; CBD = citrate-bicarbonate-dithionite extractable.

Depth below surface (cm)	pH	%C	%N	%S	$BaCl_2$ Ca mmol kg^{-1}	AAO Fe mmol kg^{-1}	CBD Fe mmol kg^{-1}
	SS zone						
0–19	2.9	5.2	0.3	2.4	22	212	11
19–38	2.7	4.7	0.3	2.3	20	228	10
38–50	2.8	5.2	0.4	1.3	19	201	15
50–66	4.3	33.3	1.8	2.6	33	110	14
66–89	5.7	40.4	1.8	2.8	58	44	5
	TS zone						
0–27	4.7	14.1	0.8	1.9	16	152	14
27–73	3.3	8.6	0.6	2.4	14	196	11
73–89	3.6	8.6	0.7	2.2	12	298	10

environment (Mitsubishi Anero-Pack Rectangular Jar) without further alteration in order to assess the natural C-mineral associations of the bulk sediments.

In preparation for STXM-NEXAFS analysis, we used established protocols to preserve elemental speciation (Chen et al., 2014; Dynes et al., 2015). Briefly, ~ 1 mg of sediment was mixed with ~1 mL of anoxic deionized-distilled water and immediately vortexted for 5–10 s. A ~50 µL suspension droplet was immediately placed onto a Si_3N_4 window (100 nm thick), and allowed to dry (≪ 1 min) in an anoxic glovebox (N_2 atmosphere). STXM-NEXAFS data collection and analysis was performed on the 10ID-1 spectromicroscopy beamline (Kaznatcheev et al., 2007) at the Canadian Light Source, a 2.9-GeV third-generation synchrotron source, following previous methods (Chen et al., 2014; Chen and Sparks, 2015) with the addition of image sequence scan (i.e., stack) collection for the N 1s and K 2p edges. Stack datasets were collected for specific element edges in the following order: C K-edge, K L-edge, Ca L-edge, N K-edge, Fe L-edge, Al K-edge, and Si K-edge. NEXAFS Spectra were baseline corrected and normalized using Athena (Ravel and Newville, 2005). Carbon K-edge peaks were assigned as follows: aromatic C at 285.2 eV, phenolic C at 287.0 eV, aliphatic C at 287.5 eV, carboxylamides at 288.2 eV, carboxylic C at 288.5 eV, and O-alkyl C at 289.4 eV (Kinyangi et al., 2006; Wan et al., 2007; Gillespie et al., 2011; Chen and Sparks, 2015). Principal component analysis of image sequence data was carried out for carbon (Chen and Sparks, 2015). Significant components were identified based on eigenvalues, eigenimages and eigenspectra (Lerotic et al., 2005).

2.5. Porewater sampling

Porewater samples were collected at discrete depths at each vegetation zone using passive porewater samplers (i.e., peepers) in triplicate (i.e., peeper nests) modified from LaForce et al., (2000). A PVC pipe (21 cm diameter, 152 cm length) housed 9–10 cells, which hold the peepers. Peepers consisted of 13 mL polypropylene tubes fitted with a plastic cap, which contains a 0.20 µm nylon membrane and initially filled with 18 MΩ deoxygenated water. The TS zone had peepers at 9 depths (0, −3, −12, −25, −40, −50, −65, −75, −90 cm) and the SS zone had peepers at 10 depths (0, −3, −12, −25, −35, −45, −55, −65, −75, −90 cm) relative to the sediment surface as depths were chosen based on sediment profiles with at least two peepers per horizon (Fig. S1). The peepers were allowed to equilibrate for at least 10 days (LaForce et al., 2000). After equilibration, the peeper cells were removed from the housing and immediately replaced with fresh peeper cells. When removed from the housing, the peeper cells were immediately placed inside a gas impermeable container with oxygen scrubbers and sealed. The samples were placed on ice and were analyzed or preserved within two hours. Sampling occurred approximately every two weeks between 8/13/14 and 8/24/15, with a three-month hiatus between 12/15/14 to 3/27/15 when temperatures were below freezing.

During peeper sampling, each water sample was aliquoted into different tubes for various analyses by using a syringe fitted with a needle to pierce the peeper cell membrane and withdraw the 13 mL of equilibrated water sample. Occasionally sediment in the peeper cell was evident and required filtering with a 0.2 µm nylon syringe filter prior to aliquoting. For redox and pH measurements, a 2 mL sample was placed into a polypropylene tube and measured with calibrated probes within 5 minutes of removing the samples from the sealed, gas-impermeable container. Concurrently, 1 mL of sample was added to a mid-range sulfide determining reagent (8 g N N-dimethyl-*p*-phenylenediamine and 8 g $FeCl_3$ in a 50% HCl solution) and solution was allowed to sit for at least 20 minutes and was then measured at 667 nm in accordance with the Cline method within 24 hours (Cline, 1969). Samples that were out of range were diluted further with deoxygenated water until it was within the range of the spectrophotometer (Reese et al., 2011). Additionally, 0.5 mL of sample was used for Fe(II) analysis using the ferrozine method (Stookey, 1970). Total Fe was obtained using microwave plasma-atomic emission spectrometry (MP-AES, HP 4100) with 5 mL of sample after 1:1 dilution and acidification with 2% trace metal grade nitric acid. At least 1 mL and 3 mL of sample, respectively, were frozen in separate tubes to measure anions via ion chromatography (IC) and dissolved organic carbon (DOC) via TOC analyzer. DOC samples were diluted after thawing in a 1:5 ratio with 18 MΩ water and analyzed (Elementar Vario-TOC cube), and the IC samples were diluted in a 1:3 ratio after thawing.

Nitrate, sulfate and phosphate were separated on an AS18 column equipped with an AG18 guard column in gradient elution mode with 20 mM KOH eluent from 0 to 13.5 min and a ramp to 45 mM from 13.5 to 16 minutes and analyzed by IC with electrical conductivity detection (Dionex DX-500). Conductivity was also measured on select samples (Thermofisher Orion STAR A322).

2.6. CO_2 and CH_4 Efflux

Measurements of CH_4 and CO_2 efflux were performed using a Los Gatos Research Ultraportable Gas Analyzer (LGR-UGA) using the static chamber method as described in previous studies (Pearson et al., 2016; Warner et al., 2018). Twelve PVC rings (10 cm in diameter) were inserted into the sediment at the TS and SS zones, 6 per zone, and arranged such that they were adjacent to the peeper nests and 180 degrees away from foot traffic in the marsh (Fig. 1). No samples were taken until at least 2 weeks after the placement of the rings to allow the area around the rings to recover from the installation. The rings remained in the surface sediments throughout the campaign.

During sampling, a PVC static chamber was placed onto the fixed ring, and the chamber was connected to the LGR-UGA with gas-tight tubing for 3 minutes to measure changes in concentrations of CO_2 and CH_4. Field measurements were taken bimonthly between June 2014 and September 2015 except for a hiatus during the winter months (12/15/14 to 3/27/15), and were more intensely sampled during the spring thaw in March 2015 (weekly for four weeks). These measurements always occurred within an hour of low tide. Surface sediment temperature was measured concurrently using an infrared thermometer (Arctic Star AR550). Efflux of CO_2 and CH_4 (GHG flux) was calculated as previously done (Pearson et al., 2016; Warner et al., 2018) using the following equation:

$$GHG\ \ Flux = \frac{\delta c}{\delta t} * \frac{V}{S} * \frac{P}{RT} \quad (1)$$

where $\frac{\delta c}{\delta t}$ is the mole fraction of the GHG in μmol mol^{-1} over time (s), V is the volume of the chamber (0.0011 m^3), S is the surface area enclosed by the chamber (0.0081 m^2), P is the atmospheric pressure (assumed to be 101.325 kPa), R is the universal gas constant (8.3 × 10–3 m^3 kPa mol^{-1} K^{-1}), and T is the sediment temperature at time of measurement (K). The change in concentration of GHG over time, or $\frac{\delta c}{\delta t}$, was calculated by fitting a linear regression for CH_4 and CO_2 throughout each measurement (after discounting 30 s as a dead-band). Only values where $r^2 > 0.85$ and $p < 0.05$ were used for flux calculations per standard protocols (Petrakis et al., 2017). All efflux values from SS or from TS zones were averaged together (n = 6 per location, Fig. 1) for each sampling date.

2.7. CO_2 and CH_4 Depth Profiling

In order to address spatial heterogeneity of GHG production vertically in the sediments, depth profiles of CH_4 and CO_2 concentrations were measured from July 2015 to August 2015 using a passive gas sampling profiler (Fig. S2). Gas-permeable silicone tubes (12.7 mm inner diameter and 3.175 mm-thick, (Jacinthe and Groffman, 2001) were placed inside a 2.34 cm × 91.4 cm polypropylene sheet with rectangular through holes cut out at 4 discrete depths relative to the sediment surface based on the horizonation for each zone (Fig. S1). One profiler was made for each zone and the depths were −17.5, −30, −50, −68 cm for TS; and −15.5, −40, −56, and −70 cm for SS. Each silicone tube was 23.5 cm long and was attached to gas-tight vinyl tubing on each end by a corrosion-resistant elbow joint. Each joint was made gas- and water-tight with silicone sealant and allowed to dry and harden prior to deployment at the field site. Barbed three-way valves were attached on one end of each of the vinyl tubes and a barbed two-way valve was attached to the other vinyl tube end. Gas-tight Teflon tubing was attached to one of the barbs on the three-way valve for ready coupling to the LGR-UGA with push-to-connect fittings, and Teflon tubing was also attached to the two-way valve barbed for ready coupling to a gas-tight bladder bag of N_2. The apparati were buried at each zone (Fig. 1) and allowed to equilibrate with the sediments for two weeks before initial measurements were made. During sampling, the LGR-UGA and N_2 bladder bag were connected to opposite ends, and the valves were opened to allow accumulated gas to flow into the LGR-UGA for measurement. Concentrations of CH_4 and CO_2 were measured until a sharp drop in concentration was observed, indicating the N_2 had cleared the chamber of CH_4 and CO_2. After sampling, the valves were closed to ensure both an air- and water-tight system. This was repeated at each depth at each zone during weekly sampling from 7/13/15–8/12/15. The LGR-UGA's high limit of detection was 892 μM (20,000 ppm) for both GHGs, and values over this limit were recorded as >892 μM.

2.8. Hydrological Measurements

A monitoring well was placed within 3 m of each peeper nest at each zone (Fig. 1). Monitoring wells were constructed of a 152 cm PVC pipe with 91 cm slotted well screen at the bottom of the well (3.12 cm diameter, Atlantic Screen Manufacturing, Inc.). The maximum screened depths for all wells ranged from 99-131 cm with screens extending 91 cm above the bottom of the well. The soil bores were made using a hand auger. The well annulus was filled with sand over the length of the screen and the upper portion filled with mud. A conductivity, temperature, and depth (CTD) sensor (Aqua TROLL 200 Data Logger) was deployed in the well approximately in the middle of the well screen. A pressure transducer (Baro-Diver) was installed at TS to record the atmospheric pressure, and these data were used to calculate water table elevation for both zones according to the following equation:

$$H = \frac{P_{obs} - P_{Atm}}{\rho g} \quad (2)$$

where P_{obs} is the pressure recorded by the CTD, P_{atm} is the atmospheric pressure, ρ is the water density and g is gravity. The elevation is given relative to marsh surface at each well, determined by measuring the water table depth manually in

both wells on 9/22/15. Water table elevations at both wells were measured between 7/8/2015 and 10/6/2015 and covered the range of depths for GHG sampling.

Spring-neap tidal times were determined by using NOAA astronomical data. Where the spring tide time was defined as occurring at full and new moons and neap tides occurring during first and third quarter moons.

2.9. Statistical Analysis

Biogeochemical porewater parameters over time were compared between the two zones by averaging all depths per sampling time and using a two-tailed *t*-test where unequal variance is assumed. Standard error was calculated for each parameter where $n = 3$ for biogeochemical parameters and $n = 6$ for GHG efflux. Variance was calculated across all depths over the entire sampling period for redox values at both zones. GHG efflux from TS and SS were compared using a Mann-Whitney U test with mean-rank comparisons. All analyzes were performed using SPSS version 26.

3. RESULTS

3.1. Sediment Characteristics

Sediments from SS and TS were different and had opposite trends with depth (Table 1). All sediments were acidic but those from SS had pH < 3 down to 50 cm depth and increased to 4.3 and 5.7 down to 90 cm. In contrast, sediments from TS were less acidic at the surface with pH 4.7 and acidity increased with depth with pH ranging 3.3 to 3.6 down to 89 cm depth (Table 1). At SS, percent C increased with depth and ranged 5 to 40%, percent N increased with depth and ranged 0.3 to 1.8%, and percent S was depleted at the 38–50 cm depth (1.3%) and was ~2.5% at all other depths. In contrast, percent C at TS decreased with depth and ranged 8.6 to 14%, and percent N and S were uniform with depth and were ~0.7 and 2%, respectively. TS also had coarser texture than SS likely resulting from coarse-grained sediment depositing on the levee at TS. Extractable Fe phases varied between the two locations, with SS having generally more reducible (i.e., CBD-extractable) Fe and similar poorly-crystalline (i.e., AAO-extractable) Fe, indicating that more Fe reduction may have occurred at TS particularly above 66 cm depth.

Our Fe EXAFS data show that the dominant Fe phases differ among zone locations and with depth (Table 2, Figs. S3 and S4). Pyrite is depleted at the 30 cm depth at TS relative to the surface and deeper depths. In contrast, pyrite is depleted in the surface and increases with depth at SS. These trends were also similar for goethite and are the opposite for ferrihydrite. Mackinawite was only present in the surface at SS. Siderite was nearly constant with depth and ~5% of the total in TS, but was lower at SS and decreased with depth to 50 cm before increasing to its highest value of nearly 5% of the total Fe at 70 cm depth (Table 2).

3.2. Porewater

Spatial heterogeneity in porewater chemical signatures was clearly apparent between TS and SS, as well as vertically within each zone (Fig. 3 and Fig. S5). At both TS and SS, seasonal trends in porewater redox were observed (Fig. 3a-b). Redox values across all depths and at both zones decreased during winter plant senescence and then increased during the spring and summer growing season. While both zones showed seasonal variation at all depths, the magnitude of redox values and trends with depth were distinct. The SS zone had significantly lower average redox values compared to TS over time ($p < 0.05$) (Fig. 3a-b). Redox values for SS were consistently low and nearly always negative, ranging −200 to 200 mV with depth. In contrast, redox at TS tended to decrease with depth, with the highest redox value of 575 mV recorded at the sediment-air interface and the lowest of −118 mV recorded at depth. This trend was more prevalent during the growing season (May-September). Redox values decreased with depth during the growing season but were more uniform during late fall and winter sampling. The TS zone had an order of magnitude higher variance in redox with depth compared to SS (18581 and 4763, respectively), with average surface porewater redox values ranging widely from 0 to 600 mV, and deeper redox values more narrowly averaged from ca. 0 to 300 mV. The TS zone had more variable

Table 2
Linear combination fitting results of first shell Fe EXAFS spectra of sediment collected from four depths at the SS zone and three depths at the TS zone at the St. Jones Reserve. FHY = ferrihydrite; GOE = goethite; MAC = mackinawite; SID = siderite; PYR = pyrite; VIV = vivianite.

X-ray sample	depth below surface (cm)	% fitted species						Reduced χ^2	R value
		FHY	GOE	MAC	SID	PYR	VIV		
SS									
a	7	45	0.3	19	2.2	18	14	1.4	0.20
b	30	48	3.2	-	1.2	22	26	1.2	0.21
c	50	38	8.5	-	0.9	26	26	1.3	0.20
d	70	33	13	-	4.9	38	11	2.1	0.19
TS									
A	10	33	13	-	4.9	38	11	2.1	0.19
B	30	45	9.3	-	4.4	19	22	1.5	0.27
C	80	39	9.3	-	4.4	33	14	1.5	0.20

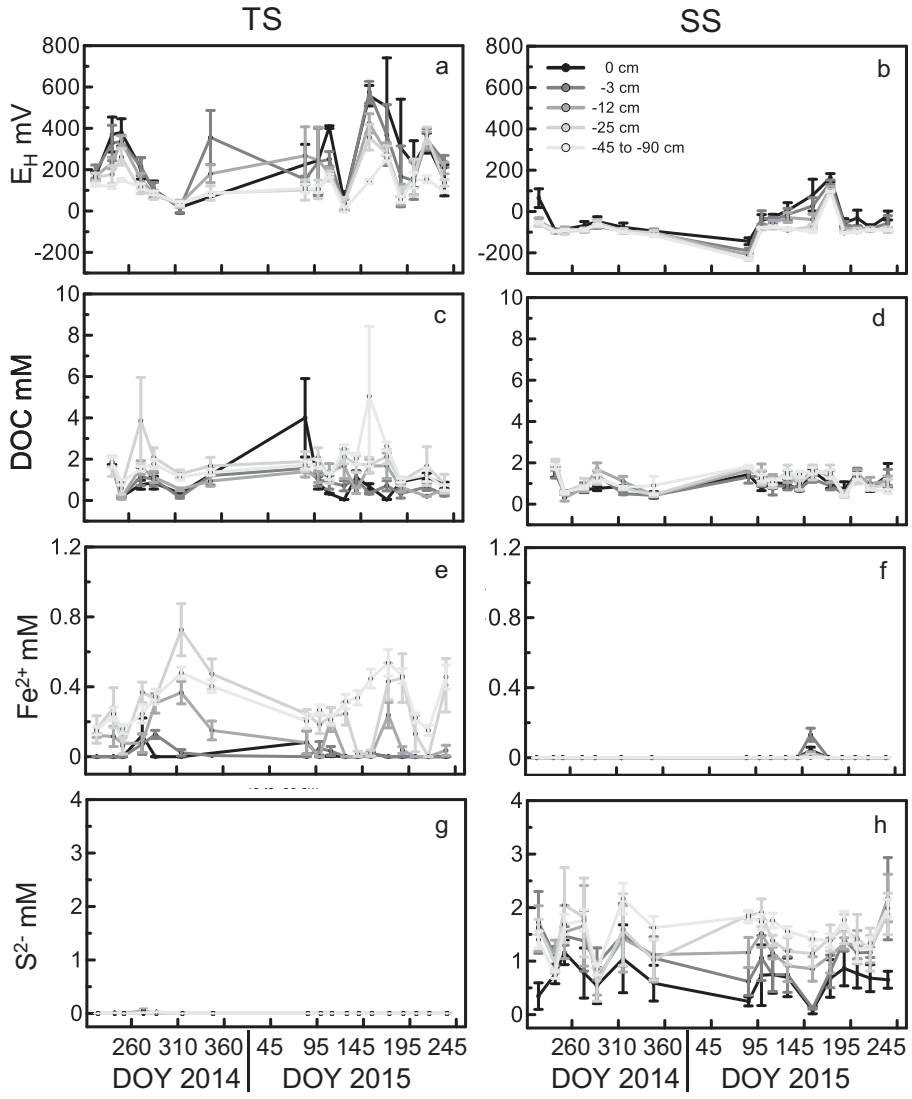

Fig. 3. Average (±SE, $n = 3$) porewater redox potential (a, b), DOC (c, d), ferrous iron (e, f), and sulfide (g, h) measured in 2014–2015 for both TS (a, c, e, g) and SS (b, d, f, h) zones.

pH both with depth and over time compared to SS (Fig. S5-a-b). The SS location was consistently between a pH of 6 and 7, whereas TS had variation near the surface, ranging from 3.5 to 7.6.

The TS zone has more variable DOC both with depth and over time compared to SS (Fig. 3c-d). Concentrations ranged from non-detectable to 8 mM at TS. In contrast, SS exhibited little variation in DOC concentration with both depth and time with values ranging from non-detectable to 2 mM.

The TS and SS zones differed greatly in the magnitude and speciation of Fe and S compounds in porewater (Fig. 3-e-h and Fig. S5c-f). Total Fe at TS was as high as 1.5 mM and increased with depth (Fig. S5e) whereas total Fe at SS was rarely detectable (Fig. S5f) despite similar amounts of CBD- and AAO-extractable iron (Table 1). Similar trends were observed with Fe(II), with concentrations up to 1.0 mM at TS and almost always non-detectable at SS (Fig. 3e-f). At TS, total Fe concentrations equaled Fe (II) concentrations at depth indicating that all the iron present was reduced at depth below −12 cm.

In contrast to Fe, concentrations of S compounds at SS were higher than at TS. Sulfide concentrations were non-detectable at TS (Fig. 3g) but were detectable at all depths at SS ranging 0.10 to 2.2 mM and tending to increase with depth (Fig. 3h). Sulfate concentrations varied with depth throughout the year, and ranged from non-detectable to 9.0 mM at TS but ranged 3.0 to 18 mM at SS (Fig. S5c-d).

3.3. CO_2 and CH_4 Efflux

Differences in the ranges and daily average of CO_2 and CH_4 were observed between the two locations (Fig. 4). At TS, CH_4 efflux ranged from −0.0002 to as high as 3.04 μmol m^{-2} s^{-1} with an average daily efflux of 9.4 (±20) mmol m^{-2} d^{-1}, and CO_2 efflux ranged from −0.5 to

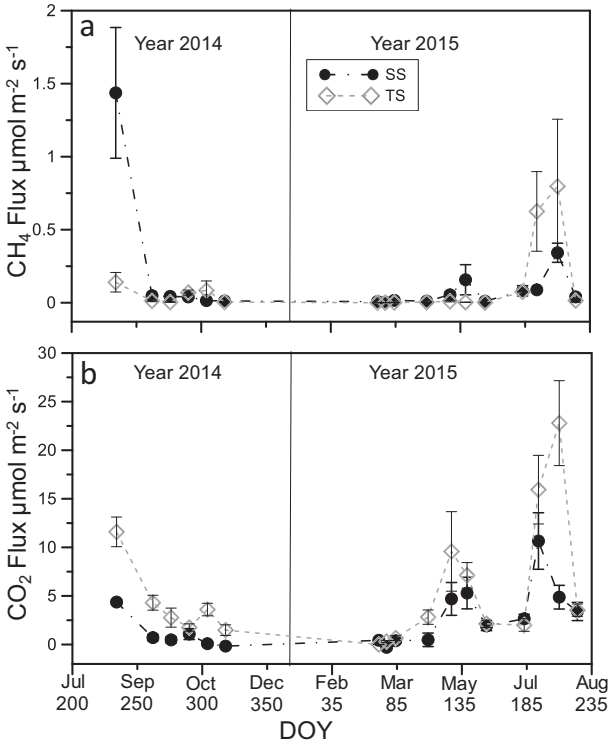

Fig. 4. Average (±SE, $n = 6$) flux of CH_4 (a) and CO_2 (b) from a nest of 6 static flux chambers at the TS (open symbols) and SS (closed symbols) vegetation zones.

as high as 42.2 µmol m^{-2} s^{-1} with an average daily efflux of 469 (±538) mmol m^{-2} d^{-1}. At SS, CH_4 efflux ranged from 0 to as high as 2.5 µmol m^{-2} s^{-1} with an average daily efflux of 12.2 (±29) mmol m^{-2} d^{-1}, and CO_2 efflux ranged from −0.9 to as high as 22 µmol m^{-2} s^{-1} with an average daily efflux of 208 (±248) mmol m^{-2} d^{-1}.

There were distinct seasonal trends in efflux of both CH_4 and CO_2 at both locations (Fig. 4). The highest efflux of CH_4 and CO_2 at both locations was observed during the middle of the summer growing seasons and declined to near zero during plant senescence in the late fall and winter (Fig. 4). Efflux of CO_2 was consistently higher for TS compared to SS, whereas the pattern for CH_4 was less clear. Efflux of CH_4 spiked in July-September at both locations for both years, yet the magnitude differed for each year with SS having a higher CH_4 spike (up to ~2.5 µmol m^{-2} s^{-1}) than TS in 2014, and the converse was observed in 2015 (Fig. 4a). A Mann-Whitney U test revealed that efflux of CO_2 was statistically significantly higher at TS ($U = 2876$, $p < 0.0001$), whereas efflux of CH_4 was statistically significantly higher at SS ($U = 2173$, $p = 0.002$) over the study period.

3.4. Water Table Elevations and CO_2 and CH_4 Production with Depth

We observed large differences in water table elevations, oscillations, and periods of land surface inundation between the two zones (Fig. 5a). The TS and SS locations had significantly different water levels ($p < 0.05$) over the measured time period of 8 July 2015–12 August 2015. The SS location exhibited daily tidal variations in water level, whereas TS exhibited both daily tidal variation in water level as well as larger variation over longer time scales associated with the spring-neap cycle (Fig. 5a). The water level at SS ranged from ca. −5 cm to as high as +18 cm relative to the marsh surface, and sediments were usually completely saturated. In contrast, water level at TS ranged from −25 cm to +10 cm with distinct periods of unsaturation down to −25 cm depth (Fig. 5a).

Depth profiles of CO_2 and CH_4 concentrations taken on 5 different days over the spring-neap tidal cycle show an apparent build-up of both CH_4 and CO_2 concentrations in the subsurface at both zones that varied in location and magnitude and at times reached the upper limit of detection (892 µM) of the instrument (Fig. 5b-e). At TS, CH_4 concentrations were low (<100 µM) at the near-surface sampling depths and increased with depth to at least 892 µM (Fig. 5b). As the water table elevation decreased from nearly 0 to −25 cm (Fig. 5a), CH_4 concentrations at depths >50 cm increased from <100 to at least 892 µM and decreased again to 300–600 µM as the water table elevation fluctuated (Fig. 5a-b). In contrast, CO_2 concentrations at TS were higher than for CH_4 and ranged from 209 to >892 µM. For almost all sampling dates, CO_2 concentration was at least 892 µM at −30 cm and below except for one sampling point shown in orange at −50 cm depth at TS (Fig. 5c).

Both the CH_4 and CO_2 depth profiles at SS differed from TS (Fig. 5b-e). During times of prolonged inundation at SS, CH_4 concentrations were high in the near-surface depths (within −20 cm) and ranged ca. 300 to 700 µM (Fig. 5a and d, red and blue). In contrast, during times of water table draw down, CH_4 concentrations at SS were non-detectable within −20 cm (Fig. 5a and d, orange and yellow). Despite differences in near-surface concentrations, CH_4 levels increased with depths of −40 cm and below regardless of the tidal cycle and ranged ca. 300 to at least 892 µM (Fig. 5d). The CO_2 concentrations at SS tended to be lower than at TS for the near-surface depths, but they were similar between zones below −40 cm depth (Fig. 5c and e).

3.5. STXM-NEXAFS

To better understand the C-mineral associations of the bulk sediments as potential factors that contributed to differences in C dynamics between zones, we examined sediment chemistry at 50 and 56 cm depth with STXM-NEXAFS. Principal component analyses (PCA) of the STXM-NEXAFS data revealed three components for each sample, but these components differed among zones (Fig. 6 and S6-7). In TS there were three components, but each had relatively uniform C speciation with predominant C K-edge NEXAFS peaks indicating the presence of aromatic and carboxylic C in all components (Fig. 6 and S6). In contrast, the PCA of the sediment sample from SS revealed three components that differed greatly in chemical composition with three distinct regions: C associated with biological

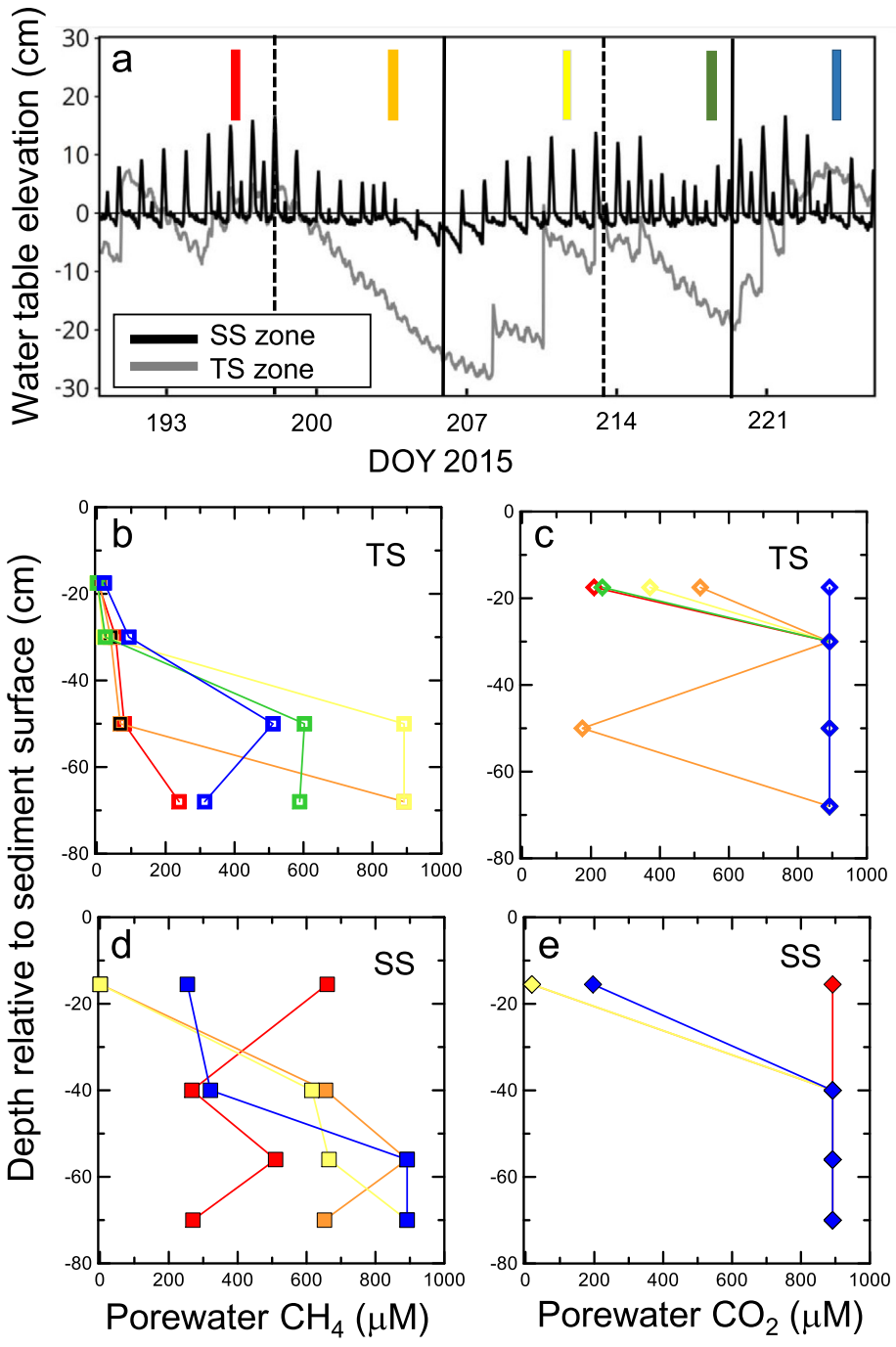

Fig. 5. Water table elevations (a) at the SS (black) and TS (grey) vegetation zones during the summer 2015 sampling period where vertical lines indicate spring (dotted) and neap (solid) tides. Zero is marsh surface elevation. Colored bars in (a) indicate when depth profiles of CH_4 (b, d) and CO_2 (c,e) concentrations in equilibrium with sediment porewater were obtained with the depth profilers at the TS (open symbols) and SS (closed symbols) zones (n = 1 per zone). Note that the maximum value obtainable by the LGR instrument was 892 μM.

material, quartz with no detectable C, and non-quartz sediment grains (Fig. 6 and S7). The SS vegetation zone showed the presence of aromatic C and carboxylic C, though with more pronounced shoulders in the phenolic and aliphatic region than in TS (Fig. 6). In particular, the biological material in SS displayed the strongest aromatic peak and the highest intensity in the phenolic and aliphatic region. Correlation analyses (Fig. S8) of the optical densi-

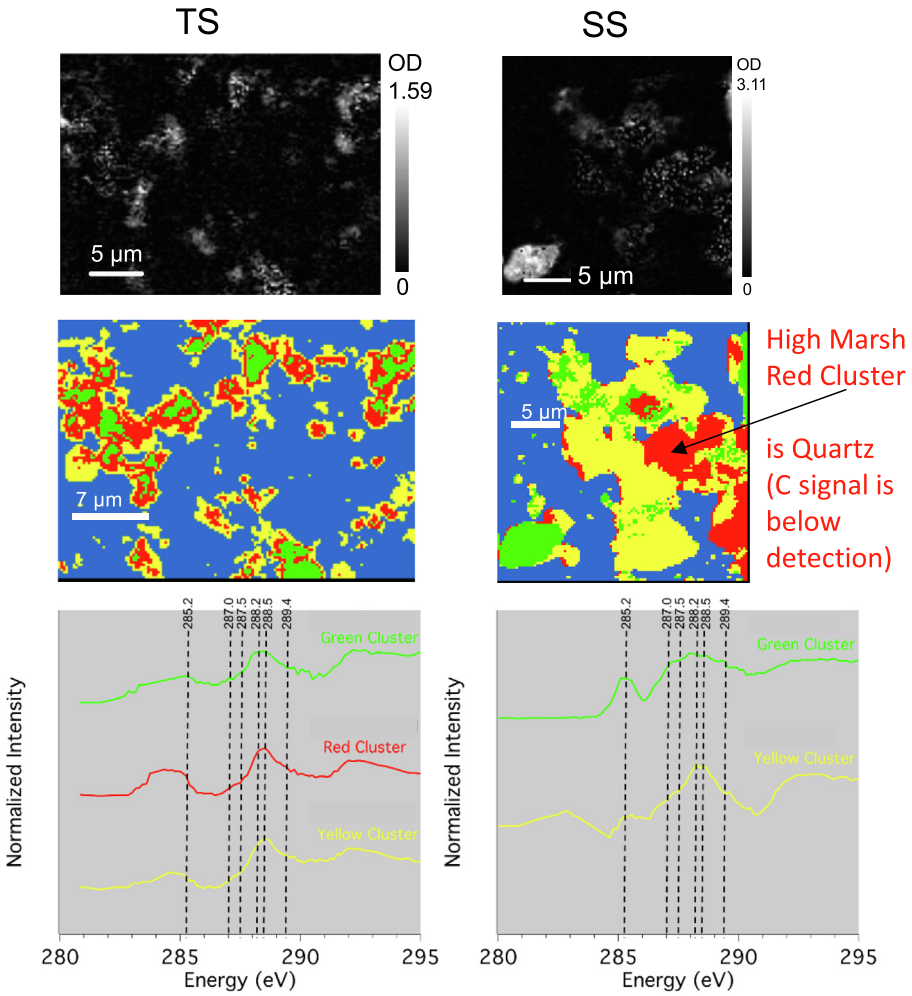

Fig. 6. STXM C images, PCA analyses and NEXAFS data of sediment collected from 50 cm depth at TS and 56 cm at SS showing three components that consisted mainly of similar C functional groups at TS and distinct C functional groups and quartz at SS. Dashed vertical lines represent aromatic C at 285.2 eV, phenolic C at 287.0 eV, aliphatic C at 287.5 eV, carboxylamides at 288.2 eV, carboxylic C at 288.5 eV, and O-alkyl C at 289.4 eV.

ties (ODs) for each element examined indicated that Ca had the strongest spatial association with C ($R^2 = 0.232$, $p < 0.0001$) compared with any other element analyzed in SS. In contrast, Fe displayed the strongest correlation with C ($R^2 = 0.284$, $p < 0.0001$) in TS.

4. DISCUSSION

Our data show that water table depth variability results in both a lateral (across the marsh) and vertical (with depth) heterogeneity in biogeochemical processes that, in turn, results in a large spatial heterogeneity of CO_2 and CH_4 production and efflux. We hypothesized that 1) vegetation zones near the tidal channel will have a greater change in water table elevation resulting in more oxidizing sediments than zones farther from the tidal channel, and 2) zones with greater change in water table elevation will have a higher rate of CO_2 and CH_4 efflux than those zones with less variation in water table elevation. Our data support both hypotheses, and we observed differences in mineral control on stored C and a pool of stored C as CO_2 and CH_4 below ~40 cm depth in sulfate-rich (up to 17 mM) porewaters. The observed CH_4 of at least 892 μM was an order of magnitude higher than reported in sulfate-rich sediments and on par with or up to 2 fold higher than those reported in freshwater systems and in marine systems below the sulfate-methane transition zone (Martens and Berner, 1977; Kelley et al., 1995; Angle et al., 2017; Xiao et al., 2018). Because these stored C-based greenhouse gases were dynamic and varied across the landscape, our results may help explain the wide ranges of C fluxes from salt marsh ecosystems, which has implications for potential land use change, weather variability and future environmental change.

4.1. Spatial heterogeneity in biogeochemical processes between zones

The landscape of the Mid-Atlantic tidal salt marsh under study in this work was similar to those described pre-

viously in Georgia having high tidal amplitudes (Nestler, 1977a; Wiegert and Freeman, 1990), which led to differences in dominant biogeochemical processes of interstitial waters across zones. The high tidal amplitude of ~2 m (Fig. 1b) led to the formation of a natural levee near the creek bank, which drove differences in redox status of interstitial waters in SS in the marsh interior and TS near the tidal channel. As described by Nestler (1977a), the natural levee near the creek bank forms as the incoming tide deposits its sediment load. This levee limits the creek water from reaching SS except in extreme high tides where creek water can overtop the levee. Therefore, the interstitial water in SS does not readily exchange with creek waters and can become strongly anaerobic (Nestler, 1977b; Nestler, 1977a). The SS zone had lower DOC concentrations that were relatively uniform with depth. This suggests little exchange with creek water, which brings in DOC with the incoming tides (Hemminga et al., 1992; Hemminga et al., 1993). We also observed strongly reducing interstitial water in SS where redox potentials were less than 100 mV down to ~1 m depth throughout the seasons and sulfide concentrations were as high as 2 mM (Fig. 3a and h). While we did not observe Fe(II) in interstitial waters (Fig. 3f), the increase in pyrite in the sediment solid phase (Table 2) suggests that as ferric oxides were reduced concurrently with sulfate (Postma and Jakobsen, 1996), ferrous sulfide minerals formed that sequestered Fe(II) from solution (Howarth et al., 1984; Morse et al., 1987). While SS experienced tidal oscillations, the water table elevation was always near the sediment surface (Fig. 5a), further enhancing strongly anaerobic sediments.

In contrast to SS, the sediments of TS were more strongly oxidizing due to relatively higher elevation of the natural levee and proximity to the tidal creek, which led to more unsaturated sediments during ebb tides particularly over spring-neap cycles. These spring-neap cycles lowered the water table level to as much as −25 cm relative to the sediment surface at TS, which provided conduits for gas exchange. Together with more exposed sediments due to higher elevation, the sediments at TS were more oxidizing than at SS (Fig. 5a). The TS location experienced more variable and higher redox potentials that never reached sulfate-reducing conditions down to ~1 m depth, and there was no detectable sulfide in interstitial porewaters despite up to 8 mM sulfate (Fig. 3g and Fig. S5c). Instead, these porewaters contained ferrous iron that tended to increase in concentration with depth, ranging from non-detectable at the surface to ca. 0.8 mM. The lack of ferrous iron at the surface was most likely because of the outgoing tide dropping the water table elevation to below the first few surface peeper cells, which likely caused any ferrous iron in those samples to oxidize between sampling events.

Because we observed different dominant geochemistry with depth >40 cm at both zones and an order of magnitude higher %C at SS at that depth (Table 1), we explored the C chemistry of the sediment solid phase below this threshold to explore controls on C-stabilization in sediments. STXM-NEXAFS analysis revealed that the C at >40 cm depth at TS was uniformly distributed and consisted of carboxyl and carboxylamide groups, indicative of degraded C (Kinyangi et al., 2006) and was most associated with Fe. This could indicate organic matter coatings on Fe-bearing minerals that were dynamic with redox oscillations at TS (Chen et al., 2018). Fe-mineral associations with organic matter have been observed in a wide variety of soil environments and tend to dominate at acidic pH (Mikutta et al., 2006; Rasmussen et al., 2006; Wagai and Mayer, 2007; Rowley et al., 2018; Rasmussen et al., 2018; Chen et al., 2018; LaCroix et al., 2019), but there has been limited data in wetland ecosystems. A recent meta-analysis that suggests pH as the master variable for predicting SOC stocks excluded histosols and organic horizons from the analysis (Rasmussen et al., 2018). The data presented here appear to fit the model that low pH and the presence of Fe oxides exert at least partial control on C retention in near-channel marsh sediments, but likely redox exerts a stronger control (LaCroix et al., 2019).

In contrast to TS, the accumulated C at >40 cm depth at SS was heterogeneously distributed. While a cluster of this C was similar to TS showing degraded carbon with Fe association (Fig. 6, yellow cluster), another cluster of this C showed strong aromatic and phenolic C signature (Fig. 6, green cluster), which is indicative of plant-derived material (Fig. 6). The plant signature of this C suggests that some of the C at depth at SS is physically protected from degradation likely due mainly to reducing conditions that limit aerobic C oxidation (Rowley et al., 2018; LaCroix et al., 2019). In addition, the C at SS in the entire sample was correlated best with Ca, and particularly for the plant-derived C (Fig. 6 and Fig. S7); a strong Ca-C association has been observed previously in a sample from a freshwater wetland (Chen and Sparks, 2015). It is noteworthy that the Ca-C association in our study occurred in acidic sediments (pH = 4.3), which is in contrast to the general view that Ca-C control dominates at basic pH (Rowley et al., 2018; Rasmussen et al., 2018). Our findings could simply indicate that the >30% C at that depth held more Ca on exchange sites (Table 1), or it could also suggest that the cluster contains protected carbon from plant cell walls, as Ca^{2+} is well-known to bind onto the negatively-charged cell walls and provide structural stability to cell walls and membranes (Marschner, 2003). However, a partial Ca control on C stability via cation bridging by inner sphere or outer sphere complexes may also be at play (Rowley et al., 2018), particularly as these sediments had little evidence of Fe cycling. We highlight that this is an important knowledge gab and more research is needed in order to unravel these potential Ca-C associations in saline, wetland sediments.

4.2. Seasonal dynamics of GHG fluxes between zones

As we hypothesized, TS had significantly higher efflux of CO_2 but not CH_4 than SS over the sampling period. While efflux of CH_4 was generally similar for TS and SS, one sampling event in summer resulted in a pulse of CH_4 at SS likely driven by ebullition, which resulted in statistically higher efflux of CH_4 at SS over the sampling period (Fig. 4). Similar to our study, King and Wiebe (1978) also observed that CH_4 efflux from a SS location in a Georgia salt marsh was predominantly from ebullition events. The

higher magnitude of C efflux from TS is likely due to escape of trapped gases as the water table elevation dropped to as low as −25 cm and enhanced heterotrophic activity associated with higher DOC. While we did not directly measure heterotrophic activity, the nearly 3-fold higher %C in surface sediments and higher porewater DOC of TS implies more available substrate supply for maintaining microbial biomass and activity within these sediments (Table 1). In addition, there was likely more CO_2 produced in sediments at TS than at SS due to more energetically favorable metabolisms in the less reducing sediments of TS. Like King and Wiebe (1978), we also observed higher C efflux during summers. This is likely due to both enhanced DOC due to plant activity and warmer temperatures as expected in a typical temperature dependence for CO_2 production and efflux (Alperin et al., 1994; Fang and Moncrieff, 2001).

4.3. Pathways and Fate of CO_2 and CH_4 production in sediments

Because we observed highest fluxes of CO_2 and CH_4 in summer, we took a closer look at production of these gases between July-August 2015. These results revealed a large pool of stored CO_2 and CH_4 with depth >−25 cm that differed in magnitude between zones. Despite higher redox potentials favoring iron reduction at depths down to ~1 m at TS, these sediments below 40 cm depth contained 75 to >892 μM CH_4, the upper limit of detection of the LGR instrument used. Higher porewater CH_4 was observed at SS that ranged 250 to >892 μM CH_4. These values are higher than values previously reported from three sites along a tidal creek of a salt marsh near the Chesapeake Bay where values < 500 μM CH_4 down to 60 cm depth were reported (Bartlett et al., 1987). Our observed values are also 2 orders of magnitude higher than CH_4 concentrations in sediments of a tidal lagoon (Deborde et al., 2010). Our depth profiles of CH_4 are more similar to those reported for freshwater wetlands or for those reported in marine sediments below the sulfate-methane transition zone. Angle et al. (2017) reported dissolved CH_4 of up to ~400 μM in sediments down to 35 cm depth in a freshwater wetland off of the Lake Erie shore, and Kelley et al. (1995) observed dissolved CH_4 as high as 900 μM using peepers and GC detection in a tidal freshwater marsh in North Carolina. Note that in our study, the concentrations of CH_4 at depth may be even higher than 892 μM, but a different instrument with a higher range of detection would need to be used, as the LGR-UGA is designed for accurate detection of trace gas concentrations. The high values of CH_4 at depth at TS occurred when SO_4^{2-} concentrations were only has high as 6 mM, but those at SS occurred at SO_4^{2-} as high as 17 mM, which suggests differences in the pathway of methane production across the marsh platform.

Our data suggest that CH_4 was being produced at depth in both zones by different pathways, but CH_4 was either not produced at the surface when the water level elevation dropped below the sediment surface, it was consumed by methanotrophic microorganisms thriving in the surface sediments (Conrad, 2007; Trotsenko and Murrell, 2008; Knittel and Boetius, 2009; Ettwig et al., 2010; Penido et al., 2016; Ettwig et al., 2016), or it was effluxed to the atmosphere. The TS zone along the creek bank is a classic example of redox zonation where more oxidizing sediments at the surface transitioned to more reducing sediments are at depth, which supported iron reduction near the surface and CH_4 production at depth. The relatively low SO_4^{2-} concentrations (non-detect to 6 mM) and non-detectable sulfide at depth at TS indicates that CH_4 production there could have proceeded via hydrogenotrophic or aceticlastic pathways as sulfate reducing bacteria were likely not competing with methanogens for substrate. This helps to explain why CH_4 concentrations at depth at TS were similar to those reported for freshwater wetlands (Kelley et al., 1995; Angle et al., 2017). In surface sediments <20 cm depth, TS porewaters contained nearly non-detectable CH_4, which suggests that CH_4 produced at depth and diffusing upward could have been partially consumed by methanotrophs either via aerobic or anaerobic metabolisms (Trotsenko and Murrell, 2008; Knittel and Boetius, 2009). The evidence of Fe reduction in sub-oxic TS sediments and relatively high proportion of ferrihydrite suggests that CH_4 consumption could have proceeded via anaerobic methanotrophic archaea who use Fe(III) from nanoparticulate ferrihydrite an electron acceptor (Ettwig et al., 2016). Any CH_4 that was not consumed by methanotrophs could have been rapidly effluxed to the atmosphere when the water table oscillated as low as −25 cm.

In contrast to TS near the tidal channel, CH_4 production at SS in the marsh interior likely proceeded via methylotrophic methanogenesis at depth, and this CH_4 had likely slower rates of methanotrophic consumption due to more strongly reducing conditions in surface sediments. The relatively high porewater CH_4 at depths below 40 cm coincided with up to 17 mM SO_4^{2-} and 2–3 mM S^{2-}. Because sulfate reduction was occurring with methanogenesis, this suggests that methylotrophic methanogensis, where sulfate reducing bacteria do not compete for substrate, was the dominate pathway at SS, and the responsible microorganisms were active at depths as low as −70 cm relative to the sediment surface. This depth is deeper than previously reported for marine sediments where methylotrophic methanogenesis dominated in surface sediments (0–10 cm) when SO_4^{2-} was near 25 mM and transitioned to aceticlastic methanogenesis below the sulfate-methane transition zone as SO_4^{2-} approached non-detectable levels (Xiao et al., 2017; Xiao et al., 2018). The high rate of biomass burial of decaying of *S. alterniflora* tissues, which release methylamine compounds (Wang and Lee, 1994), likely contributed to the deeper extent of methylotrophic CH_4 production than in marine sediments; methylamines are known to be higher in salt marshes than in marine sediments (Fitzsimons et al., 1997). The higher porewater CH_4 at SS in the surface (0–40 cm) at SS than TS was likely because there was less energetically favorable methanotrophy (e.g., sulfate-mediated anaerobic methanotrophy) occurring in these more reducing sediments compared to TS.

Similar to CH_4, dissolved CO_2 concentrations were elevated with depth >40 cm for almost all sampling events in both zones and were variable but typically lower at the sur-

face <40 cm, particularly for TS. The only CO_2 concentration at depth that was less than detector saturation (892 μM) occurred at TS during the lowest low tide under study (Fig. 5a and c), and the only surface CO_2 concentration that was >892 μM occurred at the highest high tides under study. This suggests that CO_2 produced at depth is stored within the sediment column with limited routes for vertical diffusion due to low diffusivity when sediments are saturated, but can be flushed out during extreme low tide events nearest the tidal channels when diffusivity rates increase. Thus, the fluxes of GHGs in this ecosystem can vary in space and time due to a combination of biogeochemical and hydrological drivers.

The high concentrations of CO_2 and CH_4 at depths down to ~1 m in our study demonstrate the existence of an unquantified pool of porewater CH_4 and CO_2 in sediments of salt marshes. We computed median values of CO_2 and CH_4 at both TS and SS zones, and while they were equivalent across zones for CO_2 (892 μM), they were 20x higher at the SS zone for CH_4 (74 μM for TS and 634 μM for SS). While our data are limited to summer measurements in one marsh and may not reflect global temperate marshes, it is useful to consider the global context of these findings. Assuming an extent of 5.3 Mha of temperate salt marshes worldwide (Pendleton et al., 2012; Mcowen et al., 2017), the relative distribution of zone area in our marsh of TS (37%) and SS (63%), an estimated 1:1 solid:water ratio of the sediments, and an estimated 0.9 g cm^{-3} bulk density, we computed a conservative estimate of ~70 Gg C in salt marsh porewater to 1 m depth. Of this, ~21 Gg C is as CH_4 in SS zones and only <2 Gg C is as CH_4 in TS zones. Because most research tends to focus on areas near the tidal channel or creek bank, the high CH_4 in sulfate-rich SS zones may have been overlooked in past studies.

It is often assumed that salt marshes have a high potential for C sequestration due to sulfate reduction limiting the rates of methanogenesis (Chmura et al., 2003; Mcleod et al., 2011), but our data suggest that methylotrophic methanogenesis is responsible for high CH_4 levels in SS zones of salt marshes, which according to our calculations make up at least 60% of marsh area. Supporting this is recent work in Jiangsu, China where S. *alterniflora* invasion has resulted in higher CH_4 efflux as the microbial community shifts from hydrogenotrophic to methylotrophic methanogenesis (Yuan et al., 2019) due to release of methylamines from decaying S. *alterniflora* biomass (Wang and Lee, 1994). Importantly, this stored pool of CH_4 could be rapidly lost to the atmosphere by land use change. For example, drainage of a salt marsh will result in rapid changes of physical properties (e.g., decrease of pore water), will suddenly increase GHG diffusion rates and will result in abrupt loss of stored CH_4 and CO_2 to the atmosphere. This C pool and sensitive immediate potential loss after land use change is currently not accounted for in local-to-global wetland C inventories (Petrescu et al., 2015; Hayes et al., 2018).

5. CONCLUSIONS

By coupling geochemical, biophysical and hydrologic measurements, this study revealed different drivers and controls on C cycling depending on location in a tidal salt marsh. Despite their small area of the Earth's crust, tidal salt marshes store disproportionately high amounts of C in sediments, 1–3 orders of magnitude higher than forests and other wetland ecosystems. This stored carbon has largely been thought of as resistant to degradation and therefore stable due to low rates of carbon oxidation under reducing conditions. Our data partially support this paradigm as we observed C accumulation at depth >50 cm in sediments of salt marsh interiors, but not in sediments near tidal channels. Moreover, our data reveal at least partial mineral control of C at depth via C-Fe interactions in sediments near tidal channels, but perhaps C-Ca interactions in salt marsh interiors, but these relationships must be further explored.

Salt marshes are also assumed to have limited CH_4 production due to competition between sulfate reducing bacteria and methanogens for substrate. However, our data show that CH_4 production coincides with sulfate reduction and appears to proceed via methylotrophic methanogenesis pathway in which sulfate-reducing bacteria do not compete for substrate. Therefore, while efflux appears to be low, it should not be assumed that these ecosystems do not produce CH_4. We observed concentrations of CH_4 at depth that were higher than those observed in freshwater wetlands and marine sediments. This sediment C is prone to be lost to the atmosphere with disturbance or land-use change.

Modeling efforts that are ongoing to predict future changes to C dynamics in these systems should consider the spatial heterogeneity that exists across the landscape and with depth in these sensitive ecosystems. Future work should focus on refining predictive models to capture differences in C across marsh vegetation zones and on coupling measurements of C age with microbial activity to reveal the drivers for stored C at depth. Moreover, future research across wetlands should include (bio)geochemical information to explain spatial and temporal dynamics of GHG fluxes for future incorporation of these processes in Earth System Models (Phillips et al., 2017).

Declaration of Competing Interest

The authors declare that they have no known competing financial interests or personal relationships that could have appeared to influence the work reported in this paper.

ACKNOWLEDGEMENTS

We thank the St. Jones National Estuarine Reserve staff for access to the research site and Sandra Petrakis, Erica Loudermilk, Andrew Morris, Jessica Mann and Nicholas Kaufman for help with data collection. This project was funded by the University of Delaware College of Agriculture and Natural Resources Competitive Seed Grant Program (R.V. and A.L.S.), NOAA-DNREC (R.V. and A.L.S.), the National Science Foundation Grant No. 1759879 (H.M. and A.L.S.) and 1652594 (R.V.), the Delaware Environmental Institute (J.W.S., K.K.), and the Delaware Water Resources Program (K.K.) STXM analyses were performed at the SM beamline of the Canadian Light

Source, which is supported by the Natural Sciences and Engineering Research Council of Canada, the National Research Council of Canada, the Canadian Institutes of Health Research, the Province of Saskatchewan, Western Economic Diversification Canada, and the University of Saskatchewan. Fe EXAFS and XRD analyses were performed at the Stanford Synchrotron Radiation Lightsource, SLAC National Accelerator Laboratory, which is supported by the U.S. Department of Energy, Office of Science, Office of Basic Energy Sciences under Contract No. DE-AC02-76SF00515.

APPENDIX A. SUPPLEMENTARY DATA

Supplementary data to this article can be found online at https://doi.org/10.1016/j.gca.2020.05.013.

REFERENCES

Alperin M. J., Albert D. B. and Martens C. S. (1994) Seasonal variations in production and consumption rates of dissolved organic carbon in an organic-rich coastal sediment. *Geochim. Cosmochim. Acta* **58**, 4909–4930.

Angle J. C., Morin T. H., Solden L. M., Narrowe A. B., Smith G. J., Borton M. A., Rey-Sanchez C., Daly R. A., Mirfenderesgi G., Hoyt D. W., Riley W. J., Miller C. S., Bohrer G. and Wrighton K. C. (2017) Methanogenesis in oxygenated soils is a substantial fraction of wetland methane emissions. *Nat. Commun.*, 8.

Bartlett K. B., Bartlett D. S., Harriss R. C., Sebacher D. I. and Robert C. (1987) Methane emissions along a salt marsh salinity gradient. *Biogeochemistry* **4**, 183–202.

Bartlett K. B., Harriss R. C. and Sebacher D. I. (1985) Methane flux from coastal salt marshes. *J. Geophys. Res.* **90**, 5710–5720.

Beck M., Dellwig O., Liebezeit G., Schnetger B. and Brumsack H. J. (2008) Spatial and seasonal variations of sulphate, dissolved organic carbon, and nutrients in deep pore waters of intertidal flat sediments. *Estuar. Coast. Shelf Sci.* **79**, 307–316.

Bethke C. M., Sanford R. A., Kirk M. F., Jin Q. S. and Flynn T. M. (2011) The thermodynamic ladder in geomicrobiology. *Am. J. Sci.* **311**, 183–210.

Call M., Maher D. T., Santos I. R., Ruiz-Halpern S., Mangion P., Sanders C. J., Erler D. V., Oakes J. M., Rosentreter J., Murray R. and Eyre B. D. (2015) Spatial and temporal variability of carbon dioxide and methane fluxes over semi-diurnal and spring–neap–spring timescales in a mangrove creek. *Geochim. Cosmochim. Acta* **150**, 211–225.

Cao L., Zhou Z., Xu X. and Shi F. (2020) Spatial and temporal variations of the greenhouse gas emissions in coastal saline wetlands in southeastern China. *Environ. Sci. Pollut. Res.* **27**, 1118–1130.

Capooci M., Barba J., Seyfferth A. L. and Vargas R. (2019) Experimental influence of storm-surge salinity on soil greenhouse gas emissions from a tidal salt marsh Available at:. *Sci. Total Environ.* **686**, 1164–1172 http://www.sciencedirect.com/science/article/pii/S0048969719325860.

Chanton J. P., Martens C. S. and Kelley C. A. (1989) Gas transport from methane-saturated, tidal freshwater and wetland sediments. *Limnol. Oceanogr.* **34**, 807–819.

Chen C., Dynes J., Wang J., Karunakaran C. and Sparks D. L. (2014) Soft X-ray Spectromicroscopy Study of Mineral-Organic Matter Associations in Pasture Soil Clay Fractions. *Environ. Sci. Technol.* **48**, 6678–6686.

Chen C., Meile C., Wilmoth J., Barcellos D. and Thompson A. (2018) Influence of pO(2) on Iron Redox Cycling and Anaerobic Organic Carbon Mineralization in a Humid Tropical Forest Soil. *Environ. Sci. Technol.* **52**, 7709–7719.

Chen C. and Sparks D. L. (2015) Multi-elemental scanning transmission X-ray microscopy–near edge X-ray absorption fine structure spectroscopy assessment of organo–mineral associations in soils from reduced environments. *Environ. Chem.* **12**, 64–73.

Chmura G. L., Anisfeld S. C., Cahoon D. R. and Lynch J. C. (2003) Global carbon sequestration in tidal, saline wetland soils. *Global Biogeochem. Cycles*, 17.

Cline J. (1969) Spectrophotometric determination of hydrogen sulfide in natural waters. *Limnol. Oceanogr.* **14**, 454–458.

Conrad R. (2007) Microbial Ecology of Methanogens and Methanotrophs. In *Advances in Agronomy* (ed. D. L. Sparks). ELSEVIER ACADEMIC PRESS INC, 525 B STREET, SUITE 1900, SAN DIEGO, CA 92101-4495 USA, pp. 1–63.

Darling W. G. and Gooddy D. C. (2006) The hydrogeochemistry of methane: Evidence from English groundwaters. *Chem. Geol.* **229**, 293–312.

Deborde J., Anschutz P., Guerin F., Poirier D., Marty D., Boucher G., Thouzeau G., Canton M. and Abril G. (2010) Methane sources, sinks and fluxes in a temperate tidal Lagoon: The Arcachon lagoon (SW France). *Estuar. Coast. Shelf Sci.* **89**, 256–266.

Drabsch J. M., Parnell K. E., Hume T. M. and Dolphin T. J. (1999) The capillary fringe and the water table in an intertidal estuarine sand flat. *Estuar. Coast. Shelf Sci.* **48**, 215–222.

Dynes J. J., Regier T. Z., Snape I., Siciliano S. D. and Peak D. (2015) Validating the Scalability of Soft X-ray Spectromicroscopy for Quantitative Soil Ecology and Biogeochemistry Research. *Environ. Sci. Technol.* **49**, 1035–1042.

Ettwig K. F., Butler M. K., Le Paslier D., Pelletier E., Mangenot S., Kuypers M. M. M., Schreiber F., Dutilh B. E., Zedelius J., de Beer D., Gloerich J., Wessels H. J. C. T., van Alen T., Luesken F., Wu M. L., van de Pas-Schoonen K. T., den Camp H. J. M. O., Janssen-Megens E. M., Francoijs K.-J., Stunnenberg H., Weissenbach J., Jetten M. S. M. and Strous M. (2010) Nitrite-driven anaerobic methane oxidation by oxygenic bacteria. *Nature* **464**, 543+.

Ettwig K. F., Zhu B., Speth D., Keltjens J. T., Jetten M. S. M. and Kartal B. (2016) Archaea catalyze iron-dependent anaerobic oxidation of methane. *Proc. Natl. Acad. Sci. U. S. A.* **113**, 12792–12796.

Fagherazzi S., Wiberg P. L., Temmerman S., Struyf E., Zhao Y. and Raymond P. A. (2013) Fluxes of water, sediments, and biogeochemical compounds in salt marshes. *Ecol. Process.* **2**, 3.

Fang C. and Moncrieff J. B. (2001) The dependence of soil CO2 efflux on temperature. *Soil Biol. Biochem.* **33**, 155–165.

Fitzsimons M. F., Jemmett A. W. and Wolff G. A. (1997) A preliminary study of the geochemistry of methylamines in a salt marsh. *Org. Geochem.* **27**, 15–24.

Gillespie A. W., Walley F. L., Farrell R. E., Leinweber P., Eckhardt K.-U., Regier T. Z. and Blyth R. I. R. (2011) XANES and pyrolysis-FIMS evidence of organic matter composition in a hummocky landscape. *Soil Sci. Soc. Am. J.* **75**, 1741–1755.

Grunwald M., Dellwig O., Beck M., Dippner J. W., Freund J. A., Kohlmeier C., Schnetger B. and Brumsack H. J. (2009) Methane in the southern North Sea: Sources, spatial distribution and budgets. *Estuar. Coast. Shelf Sci.* **81**, 445–456.

Hansel C. M., Benner S. G., Neiss J., Dohnalkova A., Kukkadapu R. K. and Fendorf S. (2003) Secondary mineralization pathways induced by dissimilatory iron reduction of ferrihydrite under advective flow. *Geochim. Cosmochim. Acta* **67**, 2977–2992.

Hayes D. J., Vargas R., Alin S. R., Conant R. T., Hutyra L. R., Jacobson A. R., Kurz W. A., Liu S., McGuire A. D., Poulter B. and Woodall C. W. (2018) *Chapter 2: The North American carbon budget*. U.S. Global Change Research Program, Washington, D.C..

Hemminga M. A., Klap V. A., Van Soelen J. and Boon J. J. (1993) Effect of salt marsh inundation on estuarine particulate organic matter characteristics. *Mar. Ecol. Prog. Ser.* **99**, 153–161.

Hemminga M. A., Klap V. A., van Soelen J., de Leeuw J. and Boon J. J. (1992) Shifts in seston characteristics after inundation of a European coastal salt marsh. *Limnol. Oceanogr.* **37**, 1559–1564.

Hippe H., Caspari D., Fiebig K. and Gottschalk G. (1979) Utilization of trimethylamine and other N methyl compounds for growth and methane formation by Methanosarcina barkeri. *Proc. Natl. Acad. Sci. USA* **76**, 494–498.

Holmer M. and Kristensen E. (1994) Coexistence of sulfate reduction and methane production in an organic-rich sediment. *Mar. Ecol. Prog. Ser.* **107**, 177–184.

Howarth R. W., Merkel S. and May N. (1984). *Pyrite Formation and the Measurement in Salt Marsh Sediments* **29**, 598–608.

IPCC, 2014. Climate Change 2014: mitigation of climate change., Cambridge University Press, New York, NY.

Jacinthe P. A. and Groffman P. M. (2001) Silicone rubber sampler to measure dissolved gases in saturated soils and waters. *Soil Biol. Biochem.* **33**, 907–912.

Jones H. J., Kroeber E., Stephenson J., Mausz M. A., Jameson E., Millard A., Purdy K. J. and Chen Y. (2019) A new family of uncultivated bacteria involved in methanogenesis from the ubiquitous osmolyte glycine betaine in coastal saltmarsh sediments. *MICROBIOME*, 7.

Kaznatcheev K. V., Karunakaran C., Lanke U. D., Urquhart S. G., Obst M. and Hitchcock A. P. (2007) Soft X-ray spectromicroscopy beamline at the CLS: commissioning results. *Nucl. Instrum. Methods Phys. Res. Sect. A Accel. Spectrometers Detect. Assoc. Equip.* **582**, 96–99.

Keiluweit M., Wanzek T., Kleber M., Nico P. and Fendorf S. (2017) Anaerobic microsites have an unaccounted role in soil carbon stabilization. *Nat. Commun.*, 8.

Kelley C. A., Martens C. S., Iii W. U., Sciences M., Hall V., No C. B., Kelley A. and Martens S. (1995) Methane dynamics across a tidally flooded riverbank margin. *Am. Soc. Limnol. Oceanogr.* **40**, 1112–1129.

King G. M. (1984) Metabolism of trimethylamine, choline, and glycine betaine by sulfate-reducing and methanogenic bacteria in marine sediments. *Appl. Environ. Microbiol.* **48**, 719–725.

King G. M. and Wiebe W. J. (1978) Methane release from soils of a Georgia salt-marsh. *Geochim. Cosmochim. Acta* **42**, 343–348.

Kinyangi J., Solomon D., Liang B., Lerotic M., Wirick S. and Lehmann J. (2006) Nanoscale biogeocomplexity of the organomineral assemblage in soil. *Soil Sci. Soc. Am. J.* **70**, 1708–1718.

Kludze H. K., Delaune R. D. and Patrick W. H. (1993) Aerenchyma formation and methane and oxygen-exchange in rice. *Soil Sci. Soc. Am. J.* **57**, 386–391.

Knittel K. and Boetius A. (2009) Anaerobic Oxidation of Methane: Progress with an Unknown Process. *Annu. Rev. Microbiol.* **63**, 311–334.

Knox S. H., Jackson R. B., Poulter B., McNicol G., Fluet-Chouinard E., Zhang Z., Hugelius G., Bousquet P., Canadell J. G., Saunois M., Papale D., Chu H., Keenan T. F., Baldocchi D., Torn M. S., Mammarella I., Trotta C., Aurela M., Bohrer G., Campbell D. I., Cescatti A., Chamberlain S., Chen J., Chen W., Dengel S., Desai A. R., Euskirchen E., Friborg T., Gasbarra D., Goded I., Goeckede M., Heimann M., Helbig M., Hirano T., Hollinger D. Y., Iwata H., Kang M., Klatt J., Krauss K. W., Kutzbach L., Lohila A., Mitra B., Morin T. H., Nilsson O., Niu S., Noormets A., Oechel W. C., Peichl M., Peltola O., Reba M. L., Richardson A. D., Runkle B. R. K., Ryu Y., Sachs T., Schäfer K. V. R., Schmid H. P., Shurpali N., Sonnentag O., Tang A. C. I., Ueyama M., Vargas R., Vesala T., Ward E. J., Windham-Myers L., Wohlfahrt G. and Zona D. (2019) FLUXNET-CH $_4$ Synthesis Activity: Objectives, Observations, and Future Directions BAMS-D-18-0268.1. Available at:. *Bull. Am. Meteorol. Soc.* **0**.

Kristjansson J. K., Schönheit P. and Thauer R. K. (1982) Different Ks values for hydrogen of methanogenic bacteria and sulfate reducing bacteria: An explanation for the apparent inhibition of methanogenesis by sulfate. *Arch. Microbiol.* **131**, 278–282.

Kuivila K. M., Murray J. W., Devol A. H. and Novelli P. C. (1989) Methane production, sulfate reduction and competition for substrates in the sediments of Lake Washington. *Geochim. Cosmochim. Acta* **53**, 409–416.

LaCroix R. E., Tfaily M. M., McCreight M., Jones M. E., Spokas L. and Keiluweit M. (2019) Shifting mineral and redox controls on carbon cycling in seasonally flooded mineral soils. *Biosciences* **16**, 2573–2589.

LaForce M. J., Hansel C. M. and Fendorf S. (2000) Constructing Simple Wetland Sampling Devices. *Soil Sci. Soc. Am. J.* **64**, 809.

Lerotic M., Jacobsen C., Gillow J. B., Francis A. J., Wirick S., Vogt S. and Maser J. (2005) Cluster analysis in soft X-ray spectromicroscopy: Finding the patterns in complex specimens. *J. Electron Spectros. Relat. Phenomena* **144–147**, 1137–1143.

Liu L., Wang D., Chen S., Yu Z., Xu Y., Li Y., Ge Z. and Chen Z. (2019) Methane Emissions from Estuarine Coastal Wetlands: Implications for Global Change Effect. *SOIL Sci. Soc. Am. J.* **83**, 1368–1377.

Lovley D. R. and Phillips E. J. (1987) Competitive mechanisms for inhibition of sulfate reduction and methane production in the zone of ferric iron reduction in sediments. *Appl. Environ. Microbiol.* **53**, 2636–2641.

Magenheimer J. F., Moore T. R., Chmura G. L. and Daoust R. J. (1996) Methane and carbon dioxide flux from a macrotidal salt marsh, Bay of Fundy, New Brunswick. *ESTUARIES* **19**, 139–145.

Maher D. T., Cowley K., Santos I. R., Macklin P. and Eyre B. D. (2015) Methane and carbon dioxide dynamics in a subtropical estuary over a diel cycle: Insights from automated in situ radioactive and stable isotope measurements. *Mar. Chem.* **168**, 69–79.

Marschner H. (2003) *Mineral Nutrition of Higher Plants*, second ed. Academic Press, New York.

Martens C. S. and Berner R. A. (1977) Interstitial water chemistry of anoxic Long Island Sound sediments. 1. Dissolved gases. *Limnol. Oceanogr.* **22**, 10–25.

Masue-Slowey Y., Kocar B. D., Jofre S. A. B., Mayer K. U. and Fendorf S. (2011) Transport Implications Resulting from Internal Redistribution of Arsenic and Iron within Constructed Soil Aggregates. *Environ. Sci. Technol.* **45**, 582–588.

McKeague J. A. and Day J. H. (1966) Dithionite- and oxalate-extractable Fe and Al as aids in differentiating various classes of soils. *Can. J. Soil Sci.* **46**, 13–22.

Mcleod E., Chmura G. L., Bouillon S., Salm R., Bjork M., Duarte C. M., Lovelock C. E., Schlesinger W. H. and Silliman B. R. (2011) A blueprint for blue carbon: toward an improved understanding of the role of vegetated coastal habitats in sequestering CO2. *Front. Ecol. Environ.* **9**, 552–560.

Mcowen C. J., Weatherdon L. V., Van Bochove J.-W., Sullivan E., Blyth S., Zockler C., Stanwell-Smith D., Kingston N., Martin C. S., Spalding M. and Fletcher S. (2017) A global map of saltmarshes. *Biodivers. DATA J.*, 5.

Mehra O. P. (1958) Iron Oxide Removal from Soils and Clays by a Dithionite-Citrate System Buffered with Sodium Bicarbonate. *Clays Clay Miner.* **7**, 317–327.

Le Mer J. and Roger P. (2010) Production, oxidation, emission and consumption of methane by soils : A review. *Eur. J. Soil Sci.* **37**, 25–50.

Middelburg J. J., Nieuwenhuize J., Iversen N., Høgh N., Wilde H., De Helder W., Seifert R., Christof O., Helder W. I. M., Hogh N. and Wilde H. D. E. (2014) Methane distribution in European tidal estuaries. *Biogeochemistry* **59**, 95–119.

Mikutta R., Kleber M., Torn M. S. and Jahn R. (2006) Stabilization of soil organic matter: Association with minerals or chemical recalcitrance?. *Biogeochemistry* **77** 25–56.

Montalto F. A., Parlange J.-Y. and Steenhuis T. S. (2007) A simple model for predicting water table fluctuations in a tidal marsh. *Water Resour. Res.*, 43.

Moore T. and Dalva M. (1993) The influence of temperature and water table position on carbon dioxide and methane emissions from laboratory columns of peatland soils. *Eur. J. Soil Sci.* **44**, 651–664.

Moore T. and Roulet N. (1993) Methane flux: water table relations in northern wetlands. *Geophys. Res. Lett.* **20**, 587–590.

Morse J. W., Millero F. J., Cornwell J. C. and Rickard D. (1987) The chemistry of the hydrogen sulfide and iron sulfide systems in natural waters. *Earth Sci. Rev.* **24**, 1–42.

Van Der Nat F.-J. and Middelburg J. J. (2000) Methane Emission from Tidal Freshwater Marshes. *Biogeochemistry* **49**, 103–121.

Nestler J. (1977a) A preliminary study of the sediment hydrology of a Georgia salt marsh using Rhodamine WT as a tracer. *Southeast. Geol.* **18**, 265–271.

Nestler J. (1977b) Interstitial salinity as a cause of ecophenic variation in Spartina alterniflora. *Estuar. Coast. Mar. Sci.* **5**, 707–714.

Oremland R. S., Marsh L. M. and Polcin S. (1982) Methane production and simultaneous sulphate reduction in anoxic, salt marsh sediments. *Nature* **296**, 143–145.

Pallud C., Masue-Slowey Y. and Fendorf S. (2010) Aggregate-scale spatial heterogeneity in reductive transformation of ferrihydrite resulting from coupled biogeochemical and physical processes. *Geochim. Cosmochim. Acta* **74**, 2811–2825.

Pearson A. J., Pizzuto J. E. and Vargas R. (2016) Influence of run of river dams on floodplain sediments and carbon dynamics. *Geoderma* **272**, 51–63.

Pendleton L., Donato D. C., Murray B. C., Crooks S., Jenkins W. A., Sifleet S., Craft C., Fourqurean J. W., Kauffman J. B., Marba N., Megonigal P., Pidgeon E., Herr D., Gordon D. and Baldera A. (2012) Estimating Global "Blue Carbon{"} Emissions from Conversion and Degradation of Vegetated Coastal Ecosystems. *PLoS One* **7**.

Penido E. S., Bennett A. J., Hanson T. E. and Seyfferth A. L. (2016) Biogeochemical impacts of silicon-rich rice residue incorporation into flooded soils: Implications for rice nutrition and cycling of arsenic. *Plant Soil* **399**.

Petrakis S., Seyfferth A., Kan J., Inamdar S. and Vargas R. (2017) Influence of experimental extreme water pulses on greenhouse gas emissions from soils. *Biogeochemistry* **133**.

Petrescu A. M. R., Lohila A., Tuovinen J.-P., Baldocchi D. D., Desai A. R., Roulet N. T., Vesala T., Dolman A. J., Oechel W. C., Marcolla B., Friborg T., Rinne J., Matthes J. H., Merbold L., Meijide A., Kiely G., Sottocornola M., Sachs T., Zona D., Varlagin A., Lai D. Y. F., Veenendaal E., Parmentier F.-J. W., Skiba U., Lund M., Hensen A., van Huissteden J., Flanagan L. B., Shurpali N. J., Grünwald T., Humphreys E. R., Jackowicz-Korczyński M., Aurela M. A., Laurila T., Grüning C., Corradi C. A. R., Schrier-Uijl A. P., Christensen T. R., Tamstorf M. P., Mastepanov M., Martikainen P. J., Verma S. B., Bernhofer C. and Cescatti A. (2015) The uncertain climate footprint of wetlands under human pressure 4594 LP – 4599. Available at:. *Proc. Natl. Acad. Sci.* **112**.

Phillips C. L., Bond-Lamberty B., Desai A. R., Lavoie M., Risk D., Tang J., Todd-Brown K. and Vargas R. (2017) The value of soil respiration measurements for interpreting and modeling terrestrial carbon cycling. *Plant Soil* **413**, 1–25.

Poffenbarger H. J., Needelman B. A. and Megonigal J. P. (2011) Salinity influence on methane emissions from tidal marshes. *Wetlands* **31**, 831–842.

Postma D. and Jakobsen R. (1996) Redox zonation: Equilibrium constraints on the Fe (III)/SO4-reduction interface. *Geochim. Cosmochica* **60**, 3169–3175.

Rasmussen C., Heckman K., Wieder W. R., Keiluweit M., Lawrence C. R., Berhe A. A., Blankinship J. C., Crow S. E., Druhan J. L., Pries C. E. H., Marin-Spiotta E., Plante A. F., Schadel C., Schimel J. P., Sierra C. A., Thompson A. and Wagai R. (2018) Beyond clay: towards an improved set of variables for predicting soil organic matter content. *Biogeochemistry* **137**, 297–306.

Rasmussen C., Southard R. J. and Horwath W. R. (2006) Mineral control of organic carbon mineralization in a range of temperate conifer forest soils. *Glob. Chang. Biol.* **12**, 834–847.

Ravel B. and Newville M. (2005) ATHENA, ARTEMIS, HEPHAESTUS: data analysis for X-ray absorption spectroscopy using IFEFFIT. *J. Synchrotron Radiat.* **12**, 537–541.

Reese B. K., Finneran D. W., Mills H. J., Zhu M.-X. and Morse J. W. (2011) Examination and refinement of the determination of aqueous hydrogen sulfide by the methylene blue method. *Aquat. Geochem.* **17**, 567–582.

Reid M. C., Tripathee R., Schäfer K. V. R. and Jaffé P. R. (2013) Tidal marsh methane dynamics: Difference in seasonal lags in emissions driven by storage in vegetated versus unvegetated sediments. *J. Geophys. Res. Biogeosci.* **118**, 1802–1813.

Roulet N. T. (2000) Peatlands, carbon storage, greenhouse gases, and the Kyoto Protocol: Prospects and significance for Canada. *WETLANDS* **20**, 605–615.

Rowley M. C., Grand S. and Verrecchia E. P. (2018) Calcium-mediated stabilisation of soil organic carbon. *Biogeochemistry* **137**, 27–49.

Segarra K. E. A., Comerford C., Slaughter J. and Joye S. B. (2013) Impact of electron acceptor availability on the anaerobic oxidation of methane in coastal freshwater and brackish wetland sediments. *Geochim. Cosmochim. Acta* **115**, 15–30.

Segers R. (1998) Methane production and methane consumption : a review of processes underlying wetland methane fluxes. *Biogeochemistry*, 23–51.

Senior E., Lindstrom E. B., Banat I. M. and Nedwell D. B. (1982). *Appl. Environ. Microbiol.* **43**, 987–996.

Silver W. L., Lugo A. E. and Keller M. (1999) Soil oxygen availability and biogeochemistry along rainfall and topographic gradients in upland wet tropical forest soils. *Biogeochemistry* **44**, 301–328.

Smith K. A., Ball T., Conen K. E., Dobbiw J., Massheder J. and Rey A. (2003) Exchange of greenhouse gases between soil and atmosphere : interactions of soil physical factors and biological processes. *Eur. J. Soil Sci.* **54**, 779–791.

Stookey L. L. (1970) Ferrozine—a new spectrophotometric reagent for iron. *Anal. Chem.* **42**, 779–781.

Teh Y. A. and Silver W. L. (2006) Effects of soil structure destruction on methane production and carbon partitioning between methanogenic pathways in tropical rain forest soils. *J. Geophys. Res.* **111**, G01003.

Ticak T., Hariraju D., Arcelay M. B., Arivett B. A., Fiester S. E. and Ferguson, Jr., D. J. (2015) Isolation and characterization of a tetramethylammonium-degrading Methanococcoides strain

and a novel glycine betaine-utilizing Methanolobus strain. *Arch. Microbiol.* **197**, 197–209.

Tong C., Huang J. F., Hu Z. Q. and Jin Y. F. (2013) Diurnal variations of carbon dioxide, methane, and nitrous oxide vertical fluxes in a subtropical estuarine marsh on neap and spring tide days. *Estuaries and Coasts* **36**, 633–642.

Trifunovic B., Lule A. V., Capooci M., Seyfferth A., Moffat C. F. and Vargas R. (2018) Patterns and Drivers of Carbon Dioxide and Methane Emissions from a Temperate Salt Marsh Creek. In *AGU Fall Meeting American Geophysical Union, Washington, D.C.*, pp. B43–2928.

Trotsenko Y. A. and Murrell J. C. (2008) Metabolic aspects of aerobic obligate methanotrophy. In *Advances in Applied Microbiology* (eds. A. L. Laskin and S. Sariaslani), pp. 183–229.

Villa J. A., Ju Y., Vines C., Rey-Sanchez C., Morin T. H., Wrighton K. C. and Bohrer G. (2019) Relationships between methane and carbon dioxide fluxes in a temperate cattail-dominated freshwater wetland 0. Available at. *J. Geophys. Res. Biogeosci.*.

Wachinger G., Fiedler S., Zepp K., Gattinger A., Sommer M. and Roth K. (2000) Variability of soil methane production on the micro-scale: spatial association with hot spots of organic material and Archaeal populations. *Soil Biol. Biochem.* **32**, 1121–1130.

Waddington J. M. and Roulet N. T. (1996) Atmosphere-wetland carbon exchanges: Scale dependency of CO2 and CH4 exchange on the developmental topography of a peatland. *Global Biogeochem. Cycles* **10**, 233–245.

Wagai R. and Mayer L. M. (2007) Sorptive stabilization of organic matter in soils by hydrous iron oxides. *Geochim. Cosmochim. Acta* **71**, 25–35.

Wan J., Tyliszczak T. and Tokunaga T. K. (2007) Organic carbon distribution, speciation, and elemental correlations within soil microaggregates: applications of STXM and NEXAFS spectroscopy. *Geochim. Cosmochim. Acta* **71**, 5439–5449.

Wang X. C. and Lee C. (1994) Sources and distribution of aliphatic amines in salt marsh sediment. *Org. Geochem.* **22**, 1005–1021.

Warner D. L., Vargas R., Seyfferth A. and Inamdar S. (2018) Transitional slopes act as hotspots of both soil CO<inf>2</inf>emission and CH<inf>4</inf>uptake in a temperate forest landscape. *Biogeochemistry* **138**.

Watkins A. J., Roussel E. G., Parkes R. J. and Sass H. (2014) Glycine Betaine as a Direct Substrate for Methanogens (Methanococcoides spp.). *Appl. Environ. Microbiol.* **80**, 289–293.

Weston N. B., Dixon R. E. and Joye S. B. (2006) Ramifications of increased salinity in tidal freshwater sediments: Geochemistry and microbial pathways of organic matter mineralization. *J. Geophys. Res.* **111**, G01009.

Weston N. B., Vile M. A., Neubauer S. C. and Velinsky D. J. (2010) Accelerated microbial organic matter mineralization following salt-water intrusion into tidal freshwater marsh soils. *Biogeochemistry* **102**, 135–151.

Wiegert, R.G., Freeman, B.J., 1990. Tidal salt marshes of the Southeastern Atlantic coast: A community profile. Washington, D.C.

Wilson B. J., Mortazavi B. and Kiene R. P. (2015) Spatial and temporal variability in carbon dioxide and methane exchange at three coastal marshes along a salinity gradient in a northern Gulf of Mexico estuary. *Biogeochemistry* **123**, 329–347.

Winfrey M. R. and Zeikus J. G. (1977) Effect of sulfate on carbon and electron flow during microbial methanogenesis in Effect of Sulfate on Carbon and Electron Flow During Microbial Methanogenesis in Freshwater Sediments. *Applied Environ. Microbiol.* **33**, 275.

Wolanski E. (2007) *Estuarine Ecohydrology*, first ed. Elsevier, Oxford, UK.

Xiao K.-Q., Beulig F., Kjeldsen K. U., Jorgensen B. B. and Risgaard-Petersen N. (2017) Concurrent Methane Production and Oxidation in Surface Sediment from Aarhus Bay, Denmark. *Front. Microbiol.*, 8.

Xiao K.-Q., Beulig F., Roy H., Jorgensen B. B. and Risgaard-Petersen N. (2018) Methylotrophic methanogenesis fuels cryptic methane cycling in marine surface sediment. *Limnol. Oceanogr.* **63**, 1519–1527.

Yang S. S. and Chang H. L. (1998) Effect of environmental conditions on methane production and emission from paddy soil. *Agric. Ecosyst. Environ.* **69**, 69–80.

Ying S. C., Masue-Slowey Y., Kocar B. D., Griffis S. D., Webb S., Marcus M. A., Francis C. A. and Fendorf S. (2013) Distributed microbially- and chemically-mediated redox processes controlling arsenic dynamics within Mn-/Fe-oxide constructed aggregates. *Geochim. Cosmochim. Acta* **104**, 29–41.

Yuan J., Liu D., Ji Y., Xiang J., Lin Y., Wu M. and Ding W. (2019) Spartina alterniflora invasion drastically increases methane production potential by shifting methanogenesis from hydrogenotrophic to methylotrophic pathway in a coastal marsh. *J. Ecol.* **107**, 2436–2450.

Associate editor: Martin Novak